A global survey of radiogenic strontium isotopes in river sediments

Bayon Germain [1, *], Freslon Nicolas [1], Germain Yoan [1], Bindeman Ilya N. [2], Trinquier Anne [1], Barrat Jean-Alix [3, 4]

[1] IFREMER, Marine Geosciences Unit, Brest, France
[2] Department of Earth Sciences, University of Oregon, Eugene, OR 97403-1272, USA
[3] Université Européenne de Bretagne, F-35000 Rennes, France
[4] Institut Universitaire Européen de la Mer, Université de Bretagne Occidentale, CNRS UMS 3113, F-29280 Plouzané, France

* Corresponding author : Germain Bayon, email address : gbayon@ifremer.fr

Abstract :

Radiogenic strontium isotopes are routinely used in provenance studies, but their application to sediments is often complicated by various grain size and weathering effects, which can influence measured 87Sr/86Sr ratios. Here, we report Sr isotopic data for a large number of sediment samples (n = 61) from the world's largest rivers and other river catchments draining particular geological and climatic settings; using both clay-rich (<4 μm) and silt-size (4-63 μm) detrital fractions to re-examine the factors controlling their distribution in sediments. In agreement with previous studies, the detrital material transported by world rivers defines general inverse Nd-Sr isotope relationships, which provide further empirical evidence for the utility of radiogenic Sr isotopes in sediment provenance studies. In a novel departure, however, we show that the 87Sr/86Sr difference between paired clay- and silt-size fractions (Δ87Sr/86Sr Clay-Silt) relates to the degree of chemical alteration of river sediments, as inferred from various relationships with weathering indices, such as the CIA, WIP and Na2O/Al2O3. The weathering dependence of Δ87Sr/86Sr Clay-Silt appears to be mainly controlled by temperature. In sub-Arctic and temperate regions, river sediments systematically display positive Δ87Sr/86Sr Clay-Silt indicative of preferential alteration of biotite in soils. In contrast, in sub-tropical watersheds characterized by mean annual temperatures >20 °C, intense feldspar weathering leads to the preferential incorporation of unradiogenic Sr into secondary clay minerals; a process which results in negative Δ87Sr/86Sr Clay-Silt values. In addition to climate forcing, the degree of size-dependent Sr isotope decoupling is also shown to be dependent on the type of weathering regime in watersheds, being more pronounced in low-elevation environments (< 2000 m), where transport-limited conditions and the presence of thick soil sequences can be associated with intense silicate weathering, than in high mountain regions (> 4000 m) dominated by kinetically-limited weathering regimes.

While further studies will be required to test the validity of these conclusions at the local scale of weathering profiles, these findings suggest that combined Sr isotopic analyses of separate size fractions could be used as a new weathering proxy in sediment records, ideally complementing the conventional use of radiogenic Sr isotopes as provenance tracers. Finally, our results are also used to re-assess the mean Sr flux and 87Sr/86Sr composition of the suspended sediment exported to the ocean yearly, yielding

a global flux-weighted average of 0.7160, identical to that proposed earlier in the seminal study of Goldstein and Jacobsen (1988).

Keywords : Nd-Sr isotopes, world rivers, silicate weathering, biotite, feldspars, grain-size fractions

1. Introduction

On continents, rubidium and its [87]Rb isotope, which slowly decays to [87]Sr with a half-life of almost 50 billion years (Nebel et al., 2011), is preferentially enriched in potassium-rich crustal rocks compared to mantle-derived rocks. Over geological timescales, this process has resulted in continental rocks and soils having contrasted radiogenic [87]Sr/[86]Sr signatures (*e.g.*, Gast, 1960; Faure and Hurley, 1963; Amstrong, 1968; Dymond et al., 1974; Faure and Powell, 2012). On this principle, strontium isotope geochemistry has been used for decades in sediment provenance studies (*e.g.*, Dasch, 1969; Biscaye et al., 1971; Shaffer and Faure, 1976; Asahara et al., 1999; Walter et al., 2000; Grousset and Biscaye, 2005; Hemming et al., 2007; Franzese et al., 2009). At the mineral scale, Rb and Sr are also partitioned differently into rock-forming minerals, leading with time and radioactive decay of [87]Rb to markedly different Sr isotopic compositions (see Fig 1 for an updated compilation of Rb and Sr partition coefficient ratios in common minerals). This decoupling between Rb–Sr at the mineral scale provides a means for investigating silicate weathering processes in soils (*e.g.*, Brooks, 1968; Blum and Erel, 1995; Blum and Erel, 1997; Aubert et al., 2001; Stewart et al., 2001; White et al., 2001; Oliva et al., 2004; Négrel, 2005; Pett-Ridge et al., 2009). Silicate weathering does not affect rocks uniformly, but only particular mineral phases, hence releasing a dissolved Sr fraction with a [87]Sr/[86]Sr signature that differs from the bulk rock composition. Over the past decades, extensive work has been done on Sr isotopes in the dissolved loads of river waters (*e.g.*, Goldstein and Jacobsen, 1987; Palmer and Edmond, 1989; Palmer and Edmond, 1992; Krishnaswami et al., 1992; Négrel et al., 1993; Gaillardet et al., 1997; Viers et al., 2000; Dessert et al., 2001; Millot et al., 2002; Singh et al., 2006; Wu et al., 2009; Pearce et al., 2015). While providing information on silicate rock weathering, dissolved riverine [87]Sr/[86]Sr compositions are also strongly influenced by weathering of carbonates and other marine-derived sedimentary rocks, generally characterized by relatively uniform [87]Sr/[86]Sr compositions inherited from past oceans (*e.g.*, Veizer and Compston, 1974; Veizer, 1989;

MacArthur et al., 2012). Most of the world's largest rivers have now been characterized for radiogenic Sr isotopes (for a recent review, see Peucker-Ehrenbrink and Fiske, 2019). Comparatively, the river suspended loads and associated sediments have received less attention with regard to Sr isotopes. Following the seminal work of Goldstein and Jacobsen (1988), which reported $^{87}Sr/^{86}Sr$ data for suspended loads from rivers across North America and a few other locations worldwide, several case studies investigated the radiogenic Sr isotope geochemistry of suspended particulates, bedloads and other river-borne sediments from large river systems (*e.g.*, Douglas et al., 1995; Allègre et al., 1996; Derry and France-Lanord, 1996; Eisenhauer et al., 1999; Galy and France-Lanord, 2001; Viers et al., 2008; Singh et al., 2008; Bouchez et al., 2011; Mao et al., 2011; Garçon et al., 2014; Rousseau et al., 2019). However, its application to river suspended loads and other sediments is often complicated by the fact that measured $^{87}Sr/^{86}Sr$ ratios can reflect various grain-size and weathering effects in addition to tracing sediment provenance (*e.g.*, Biscaye et al., 1971; Eisenhauer et al., 1999; Bouchez et al., 2011; Meyer et al., 2011; Garçon et al., 2014). One major difficulty is that rubidium-rich mineral phases are commonly preferentially enriched in the finest sediment fractions, hence typically resulting in clay-size sediments being more radiogenic than coarser silty and sandy sediments (*e.g.*, Biscaye et al., 1971; Eisenhauer et al., 1999; Bouchez et al., 2011). To date, the potential of radiogenic Sr isotopes in river sediments for tracing continental weathering processes is yet to be fully explored.

In this study, we investigate the radiogenic Sr isotope composition of modern river sediments collected from various geological, tectonic and climatic settings worldwide. In contrast with soil studies, which allow detailed reconstruction of weathering processes along soil depth profiles, but are also strongly affected by local effects related to differences in bedrock composition and primary mineral assemblages, the geochemical composition of fine-grained

sediments deposited near the mouth of rivers provides insights into weathering processes at the catchment scale. Such a global approach is ideally suited for investigating the mechanisms controlling the distribution of geochemical tracers in sediments and for 'calibrating' weathering proxies against modern basin parameters (*e.g.*, Bayon et al., 2016; Bayon et al., 2018; Bayon et al., 2020a; Bindeman et al., 2019). Two different grain-size fractions were investigated: 1) the finest clay-rich (<4μm) detrital material, which includes secondary clays formed in soils during silicate weathering processes; and 2) the silt-size (4-63μm) terrigenous component, corresponding to a mixture of both primary and weathered minerals transported in the suspended particulate load (Bindeman et al., 2019). The difference between $^{87}Sr/^{86}Sr$ ratios in clay- and silt-size detrital fractions is found to display general relationships with proxies for chemical weathering intensity, but also with various basin parameters, such as temperature and relief, which altogether indicate that the size-dependent $^{87}Sr/^{86}Sr$ variability in river sediments is largely inherited from relatively recent weathering processes (i.e. at the timescale of soil formation in drainage basins).

2. Materials and methods

2.1. World river sediments and catchment characteristics

A total of 61 modern sediment samples were analysed, corresponding to either river, estuarine, or marine fine-grained sediments deposited near the mouth of rivers. Information on sampling location and depositional settings is provided in Table 1 and Table S1, respectively. Most samples were collected either manually, from recent river bank deposits, or by gravity coring, using core-tops or near-surface sediment layers. Two additional samples correspond to river suspended particulates from the Congo Basin, collected in December 2013 at the end point of the Kasai and Lualaba (Upper Congo) rivers, with a respective suspended sediment concentration of 53 and 108 mg/l (Bayon et al., 2018). All studied samples

correspond either to modern or relatively recent sediments deposited presumably during the last few centuries. Selected samples include some of the world's largest rivers (*e.g.*, Amazon, Congo, Mississippi, Nile, Yangtze, Mackenzie, Ganges-Brahmaputra), in addition to smaller river basins associated with particular geological settings, such as ancient cratons or volcanic provinces (Fig. 2). Studied samples were classified into three categories based on the lithological composition of corresponding watersheds (Table S1), following the approach described in Bayon et al. (2020a): 1) Rivers draining crystalline basements dominated by igneous, metamorphic and/or siliciclastic sedimentary rocks (n=19). This category includes those rivers flowing through diverse Precambrian regions in Africa (Niger, Congo, and their tributaries, Betsiboka), northern South America (Orinoco, and its right-bank tributaries), Canada (Churchill), Australia (Murchinson, Gascoyne, Fortescue, East Alligator), Fennoscandia (Kymiijoki, Ume, Lule), and a small river from the Hercynian Armorican Massif in France (Elorn); 2) Rivers draining volcanic provinces (n=3) in Northern Ireland (River Maine, Six Mile Water) and Indonesia (Brantas); 3) Rivers draining basins of mixed lithology dominated by sedimentary rocks, which include most of the major river systems investigated in this study (n=39). Note that three sediment samples from the Loire River were analysed in this study, collected along a 50-km transect in the river estuary, in order assess the analytical uncertainty associated with sediment sampling and preparation. Information on mean annual air temperatures (MAT) in studied watersheds was derived from the literature (*e.g.*, Pinet and Souriau, 1988) or, when unavailable, from the CLIMWAT climatic database managed by the Food and Agriculture Organization of the United Nations (FAO; http://www.fao.org/land-water/databases-and-software/climwat-for-cropwat/en/). The maximum elevation in river basins was obtained from Milliman and Farnsworth (2011), or was determined using a geographical information system (see Bayon et al., 2020a for details).

2.2. Chemical preparation

Sieved (<63 µm) bulk sediment samples were treated using a sequential leaching procedure that successively removes carbonate minerals, reducible Fe-Mn oxide fractions, and organic matter, while ensuring no partial dissolution of the residual detrital fractions (Bayon et al., 2002). Clay-rich (<4 µm) and silt-size (4-63 µm) detrital fractions were then separated from the residual detritus by centrifugation (Bayon et al., 2015). The reproducibility of our centrifuge method and its efficiency at separating < 4µm fractions from coarser silt particles was thoroughly assessed through grain size measurements using a Malvern Mastersizer 3000 laser diffraction particle size analyser. For Sr isotopes and major/trace element analyses, about 25 mg of powder samples were digested in cleaned PTFE vials using ultrapure concentrated HF (1.5 ml) and HCl (0.5 ml) solutions, left on hotplate for 5-7 days (140°C) after addition of a Tm spike. After evaporation, the dry residues were further digested in 6M HCl (2 days at 140°C), and finally taken (after drying) in sub-boiled 3M HNO_3 (2 ml) for subsequent geochemical analyses.

2.3. Sr isotopes

Strontium isotopic measurements were performed at the Pôle Spectrométrie Océan (Brest) using a Thermo Scientific Neptune multi-collector ICPMS, after Sr purification onto chromatographic columns containing 1 ml Eichrom Sr spec resin (100-150 µm mesh). After sample loading (1 ml) and subsequent addition of 3M HNO_3 (5 ml) onto the columns, the Sr fractions were collected in ultrapure (18.2 MΩ) water (4 ml). Strontium isotopic abundances were determined during one analytical session using a sample-standard bracketing technique, during which an in-house Sr standard solution (PlasmaCAL) was analysed every three samples. Potential interferences of Kr and Rb on masses ^{86}Sr and ^{87}Sr were monitored and corrected using ^{82}Kr, ^{83}Kr and ^{85}Rb, respectively. All standards and samples were prepared as

500 ppb solutions, which corresponded to a ^{88}Sr beam of ~ 40V. Mass bias corrections on Sr were made with the exponential law, using ^{86}Sr/^{88}Sr = 0.1194. Repeated analyses of a NIST-987 reference solution during the analytical session gave ^{87}Sr/^{86}Sr of 0.710250 ± 0.000009 (2 SD, n=38), identical to the reference value of 0.710250 ± 0.000012 (Weiss et al., 2005). The accuracy and repeatability of measured ^{87}Sr/^{86}Sr ratios were further assessed by analysing several replicates of a series of geological reference materials (BHVO-2; BIR-1; BCR-1; BCR-2), which all gave values and precisions in full agreement with literature data (Table 2).

2.4. Major elements and Sr and Rb abundances

The major element composition of most studied clay- and silt-size fractions, previously determined by wavelength dispersive X-ray fluorescence (WD-XRF), was already reported in Bayon et al. (2015). In this study, new major element data for an additional set of sediment samples (N=36) were determined with a Thermo Scientific Element XR sector field ICP-MS, using the following peaks (^{23}Na, ^{24}Mg, ^{27}Al, ^{31}P, ^{39}K, ^{44}Ca, ^{49}Ti, ^{55}Mn, ^{57}Fe) acquired in medium mass resolution. The Sr and Rb concentrations were also measured for all studied samples in low resolution mode, using ^{88}Sr and ^{85}Rb, respectively. Elemental abundances were calculated using the Tm addition method, following procedures described in Barrat et al. (1996) and Barrat et al. (2012). The in-run uncertainties on all measurements were better than 2%. The precision and accuracy of our data were assessed by analysing a series of geological certified reference materials having various chemical compositions (AN-G, AGV-1, BCR-1, DNC-1, DR-N, G-2, WS-E). The results obtained for these six reference materials were in full agreement with reference values from the literature (typically <8%), with precisions generally better than 10% (RSD; N=3).

3. Results

Major element concentrations of studied samples are listed in the supplementary Table S2. Measured Sr concentrations in studied clay- and silt-size detrital fractions range from 19 (Kasai) to 227 µg/g (Churchill) and from 33 (Mae Klong, East Alligator) to 290 µg/g (Churchill), respectively, with mean values of 83 and 122 µg/g (Table 1). As expected, river clays generally display higher Rb abundances (mean 142 µg/g) than silts (mean 88 µg/g), with concentrations ranging from 7 and 8 µg/g (River Maine) to 256 and 191 µg/g (Mae Klong), respectively. Both clayey and silty fractions encompass a large range of $^{87}Sr/^{86}Sr$ values: from ~0.705, for the volcanogenic sediments of Northern Ireland (River Maine, Six Mile Water) and Indonesia (Brantas), to ~0.780-0.800, for the sediments derived from the ancient cratons of Western Australia (Fortescue, Fitzroy) and Guiana (Rio Caroni and Rio Caura). The variation of the Sr isotopic composition in studied river-borne sediments can be illustrated using a (pseudo) isochron diagram, where $^{87}Sr/^{86}Sr$ ratios are plotted against Rb/Sr (Fig. 3). While $^{87}Sr/^{86}Sr$ vs. $^{87}Rb/^{86}Sr$ diagrams are routinely used in geochronological studies, typically forming linear arrays with a slope proportional to the age, Rb-Sr isochron correlations in sediments have generally no direct age significance due to the strong mobility of both Rb and Sr during weathering (*e.g.*, Douglas et al., 1995). In this study, except for a few samples derived from rivers draining Precambrian terranes (Fitzroy, Narva, Nelson; Fig. 3a), the clay-rich and silt-size detrital fractions derived from multi-lithological catchments display a weak mixing relationship ($R^2 = 0.38$) between a mantle-derived endmember, corresponding to those samples collected from volcanic provinces and characterized by low $^{87}Sr/^{86}Sr$ and Rb/Sr ratios, and crustal materials having higher Rb/Sr and more radiogenic Sr isotopic compositions. Compared to those mixed/sedimentary basins, which typically integrate the lithological and chemical diversity of the upper continental crust, the sediments derived from ancient crystalline basements generally display higher $^{87}Sr/^{86}Sr$ ratios for any

given Rb/Sr, reflecting the presence of older bedrocks in corresponding watersheds (Fig. 3a). As shown previously (*e.g.*, Eisenhauer et al., 1999), the observed relationship defined by multi-lithological catchments in Fig. 3a is mostly controlled by the average age of the upper continental crust drained in river catchments, but also by a grain-size effect, by which clay-size fractions generally display higher $^{87}Sr/^{86}Sr$ and Rb/Sr ratios than corresponding silt fractions (Fig. 3b). Note however that a few samples display an opposite Rb-Sr isochron relationship (*e.g.*, Congo, Mackenzie, Murchinson, Red River), with silt-size fractions being characterized by high Rb/Sr ratios and more radiogenic Sr isotopic compositions compared to corresponding clay fractions (Fig. 3b).

When plotted against corresponding neodymium (Nd) isotopic compositions (expressed here as ε_{Nd}), a well-established tracer of provenance in sediments (*e.g.*, Grousset et al., 1988), our $^{87}Sr/^{86}Sr$ data for river sediments display typical curved (hyperbolic) relationships (Fig. 4a). To a large extent, the inverse correlation between $^{87}Sr/^{86}Sr$ and ε_{Nd} in the detrital material transported by world rivers reflects variations in the Sm/Nd and Rb/Sr ratios of source rocks having different geological ages on continents (*e.g.*, Goldstein, 1988; Goldstein and Jacobsen, 1988; Fig. 3a). In this study, this general relationship brings additional evidence for the utility of Sr isotopes as provenance tracers in sediment records. Note that it is mostly apparent for sediments from river catchments draining mixed/sedimentary rock formations, with correlation coefficients (R^2) of 0.71 and 0.64 (excluding the sample from the Nelson River) for clay-rich and silt-size fractions, respectively. Considered separately, the detrital fractions derived from ancient cratons and other crystalline catchments exhibit weaker correlations between $^{87}Sr/^{86}Sr$ and ε_{Nd} (with R^2 of 0.23 and 0.40 for clay- and silt-fractions, respectively; Fig. 4a), hence suggesting that the original Sr isotopic provenance signal in these sediments may be overprinted by weathering processes.

As commonly reported in previous studies (*e.g.*, Biscaye et al., 1971; Eisenhauer et al., 1999), the clay-size fractions investigated here are commonly more radiogenic (i.e. having higher $^{87}Sr/^{86}Sr$ ratios) than corresponding coarser sediment fractions. Nevertheless, among our series of sediments (n=61), a total of 11 samples, including the Congo, Kasai, Nile, Mackenzie, Red River and Chao Phraya rivers, are characterized by clays being less radiogenic than corresponding silts (Table 1; Fig. 4b). The observed $^{87}Sr/^{86}Sr$ difference between paired clay- and silt-size fractions, defined from hereafter as $\Delta^{87}Sr/^{86}Sr_{Clay-Silt}$, appears to be larger in sediments derived from ancient crystalline basements characterized by unradiogenic Nd isotopic signatures ($\Delta^{87}Sr/^{86}Sr_{Clay-Silt}$ ranging from -0.019 to +0.028; with a mean value of 0.003 ± 0.013; 1 SD; n=19), compared to those from mixed/sedimentary basins (from -0.011 to +0.015; mean 0.005 ± 0.005; n=39) and volcanic provinces (mean 0.002 ± 0.002; n=3) associated with more radiogenic Nd isotopic compositions (Fig. 4b). Note that the analyses of the Loire River samples (N=3; Table 1) give a mean $\Delta^{87}Sr/^{86}Sr_{Clay-Silt}$ of 0.0074 ± 0.0004 (2 SD), which can be taken, to a first approximation, as an estimated uncertainty on given $\Delta^{87}Sr/^{86}Sr_{Clay-Silt}$ values in this study.

4. Discussion

4.1. Significance of measured $^{87}Sr/^{86}Sr$ ratios in clay- and silt-size fractions

As will be discussed in the following sections, our main working hypothesis is that the observed $^{87}Sr/^{86}Sr$ differences between paired clay- and silt-size fractions ($\Delta^{87}Sr/^{86}Sr_{Clay-Silt}$) mostly reflect the type and intensity of silicate weathering in river catchments. One alternative hypothesis would be that the degree of Sr isotope grain-size decoupling in river sediments is mainly controlled by the average bedrock age of corresponding catchments. As suggested previously (Eisenhauer et al., 1999), this would imply that the slope of the pseudo-isochrons

defined by paired clay- and silt-size fractions in Fig. 3 is directly dependent on the mean

bedrock age. This hypothesis can be directly tested using Nd isotopes, because the Nd

isotopic composition of suspended particulates and river sediments strongly correlates with

the average bedrock age of corresponding catchments (Goldstein and Jacobsen, 1988;

Peucker-Ehrenbrink et al., 2010). Here, the evidence that no particular relationship can be

drawn when plotting the slope of these pseudo-isochrons with corresponding ε_{Nd} ratios for

both clay- and silt-size fractions ($R^2 \sim 0.02$; graph not shown here) suggests that this

hypothesis is unlikely to account for all of the observed size-dependent decoupling of Sr

isotopes in studied river sediments. In addition to the mean bedrock age of river catchments,

several other parameters could also partly influence the distribution of radiogenic Sr isotopes

in studied size fractions. These factors are briefly reviewed below.

First, while our centrifuge method aims at separating weathered clays from primary detrital

minerals in river sediments, this approach is not quantitative, resulting in partial admixtures of

weathered and primary mineral phases in both clay-rich and silt-size fractions, with possible

influence on measured $^{87}Sr/^{86}Sr$ ratios. As a consequence, an important pre-requisite to

interpreting Sr isotopic data in separate size fractions is to estimate the contribution of

weathered *versus* primary detrital signatures in each studied sample. This can be done using

the total water contents previously determined by thermal conversion elemental analysis on

the same suite of samples (Bindeman et al., 2019; Table S3). While the primary detrital

silicate component of river sediments is mostly anhydrous (mean 1.8wt% H_2O), phyllosilicate

clay minerals display water contents ranging from ~14% (kaolinite), ~11% (smectite, chlorite)

to ~6% (illite) (Bindeman et al., 2019). Using clay mineral data previously determined on the

same < 4μm fractions (Bayon et al., 2015), a theoretical water content can be computed for

clay mineral assemblages in each sample, which, when compared to corresponding

(measured) H_2O wt% values, can provide an estimate for the proportion of primary detrital minerals (see details in Table S3). These calculations indicate that primary minerals generally account for less than 20 wt% in studied < 4μm fractions (average ~9%), except for three samples from the Nelson (~45%), Amu Darya (~42%) and Fraser (34%) rivers (Table S3). Apart from these latter samples, this means that the Sr isotopic composition of studied clay-size fractions is largely dominated by weathered minerals, even if considering that primary minerals are preferentially enriched in Sr relative to weathered products (by a factor of ~ 1.6 ± 0.7, as inferred from the average Sr concentrations for studied clay-rich and silt-size fractions; Table 1). Similarly, the proportion of weathered mineral phases in river silts can be estimated using measured total water contents, indicating that weathered minerals can account for up to 30 wt% in these fractions (Table S3). Amongst studied river silts, a few samples appear to host substantially higher amounts of weathered minerals (Table S3). This is the case for the Mackenzie (34%), Amazon (35%), Caura (60%), Murray-Darling (68%), Congo (71%), and Niger (74%) rivers. In these particular samples, the presence of clays could reflect either incomplete particle size separation during our centrifuge procedure and/or, for the case of marine sediment samples (i.e. Amazon, Mackenzie, Congo, Niger, Murray-Darling), the presence of non-disintegrated (hence > 4μm) faecal pellets containing fine clay material. Using a simple mass balance model, these estimates can be used to compute a theoretical $^{87}Sr/^{86}Sr$ silt ratio, corrected from the presence of weathered minerals (Table S3). Except for the Murray-Darling silt fraction, for which the corrected Sr isotopic composition returns an unrealistically low value (0.6742) that departs significantly from the measured ratio (0.7216), the observed $^{87}Sr/^{86}Sr$ difference between corrected and measured values in all other samples is systematically lower than ~ 0.0015. Importantly, this difference is small (~ 3%) compared to the observed range of $\Delta^{87}Sr/^{86}Sr_{Clay-Silt}$ in this study (~0.047), meaning that the potential presence of weathered material in studied silt fractions should not affect any of the

interpretations that will be drawn in the sections below, when discussing about the factors controlling the variability of $\Delta^{87}Sr/^{86}Sr_{Clay\text{-}Silt}$. Note however that the silt fraction from the Murray-Darling sample will be discarded in the discussion below.

Furthermore, the degree of size-dependent decoupling of Sr isotopes in river sediments could also reflect a source effect, in the case where clay- and silt-size detrital particles are derived from distinct source rocks. For instance, such source effect could possibly relate to the presence of fine atmospheric particles derived from distant dust source regions (*e.g.*, Probst et al., 2000; Pett-Ridge et al., 2009). Additionally, recent studies based on Nd isotopes have documented the preferential presence of radiogenic volcanogenic particles (*i.e.* characterized by relatively high ε_{Nd} signatures) in the finest size fractions of river suspended loads (*e.g.*, Garçon and Chauvel, 2014; Bayon et al., 2020). To investigate whether such effect could partially account for the observed size-dependent Sr isotope decoupling in the rivers draining mixed lithologies, $\Delta^{87}Sr/^{86}Sr_{Clay\text{-}Silt}$ is plotted against $\Delta\varepsilon_{Nd\ clay\text{-}silt}$, i.e. the difference of Nd isotopic compositions between the same clay-rich and silt-size fractions (Bayon et al., 2015; Fig. 5). While a few samples from multi-lithological catchments indicate $\Delta\varepsilon_{Nd\ clay\text{-}silt}$ values > 1 (*i.e.* Fraser, Nile, Mekong, Don, Mississippi, Chao Phraya and Fly) that most likely reflect the preferential contribution of radiogenic volcanogenic particles to the finest size fractions of the sediment, no particular correlation exists between $\Delta^{87}Sr/^{86}Sr_{Clay\text{-}Silt}$ and $\Delta\varepsilon_{Nd\ clay\text{-}silt}$ in studied river sediments ($R^2 = 0.02$; $p \ll 0.001$), hence suggesting the absence of any significant source effect. Previous work showed that the addition of as little as 5-10 % of young volcanogenic material could shift the Sr isotopic composition of any sediment towards significantly lower $^{87}Sr/^{86}Sr$ ratios (from *e.g.* > 0.730 to < 0.720), without affecting much its ε_{Nd} value (Goldstein, 1988). As a consequence, the potential control of fine volcanogenic particles on the observed size-dependent Sr isotope decoupling was also assessed by plotting

$\Delta^{87}Sr/^{86}Sr$ $_{Clay-Silt}$ *versus* other geochemical indices for basic source rock signatures (*e.g.*,

TiO_2/SiO_2; shale-normalized La/Gd ratios) and the percentage of volcanic rocks in studied

river catchments (Table S1). In case of any significant contribution of volcanogenic particles

in the clay-rich fractions, one would expect $\Delta^{87}Sr/^{86}Sr$ $_{Clay-Silt}$ from multi-lithological

catchments to display an inverse relationship with both TiO_2/SiO_2 and the proportion of

volcanic rocks, and a positive correlation with $(La/Gd)_N$ ratios. The absence of any particular

correlations between the above-mentioned parameters (plots not shown here) further suggests

that the presence of fine-grained volcanic detritus is unlikely to represent a dominant factor

accounting for the observed $^{87}Sr/^{86}Sr$ differences between clay-rich and silt-size fractions.

Interestingly, in Fig. 5, a few samples from ancient cratonic areas (i.e., Ume, Lule,

Murchinson, Kasai) appear to display significant size-dependent decoupling for both Sr and

Nd isotopes. While a source effect cannot be discarded in these particular samples, the

occurrence of $\Delta\varepsilon_{Nd}$ $_{clay-silt}$ variability in old crystalline catchments is likely to be caused by

incongruent silicate weathering (e.g., Öhlander et al., 2000; Bayon et al., 2015; Dausmann et

al., 2019). The effect of incongruent dissolution of silicate rocks on radiogenic Sr isotopes and

$\Delta^{87}Sr/^{86}Sr$ $_{Clay-Silt}$ will be discussed below in sections 4.2 and 4.3.

Additional source effects could also potentially relate to the dissolution of carbonaceous

sedimentary rocks and/or rainwater Sr inputs in river catchments; both known to locally

influence the Sr budget in soils (*e.g.*, Borg and Banner, 1996; Clow et al., 1997; Capo et al.,

1998). In contrast to igneous rocks, the $^{87}Sr/^{86}Sr$ composition of carbonates and other marine-

derived precipitates on continents is typically unradiogenic and relatively homogenous,

reflecting the fact that seawater chemistry has fluctuated within a limited range of low

$^{87}Sr/^{86}Sr$ values over geologic times (between ~ 0.706 to 0.710; *e.g.*, Veizer, 1989; McArthur

et al., 2001). Similarly, the Sr isotopic composition of rainwater is influenced by marine

sources and typically exhibit relatively low $^{87}Sr/^{86}Sr$ values (~ 0.706 - 0.719; see Hajj et al., 2017 for a recent review). In soils, the Sr isotopic composition of the exchangeable cation pool represents a mixture between local dissolved Sr inputs derived from bedrock weathering and atmospheric contributions associated with both dry (dust) and wet (rainfall) deposition (*e.g.*, Miller et al., 1993; Chow et al., 1997; Probst et al., 2000; Pett-Ridge et al., 2009). Presumably, the combination of both carbonate dissolution and atmospheric inputs in soils could thus be accompanied by the incorporation of unradiogenic (seawater-like) Sr upon clay mineral formation, which, in turn, would also affect measured $\Delta^{87}Sr/^{86}Sr$ $_{Clay-Silt}$ values in corresponding river sediments. In this study, we did not observe any particular differences for $\Delta^{87}Sr/^{86}Sr$ $_{Clay-Silt}$ between catchments influenced by intense carbonate weathering (*e.g.*, Seine, Rhine, Northern Dvina; Gaillardet et al., 1999a) and those dominated by silicate weathering (*e.g.*, Orinoco, Parana, Niger, Amazon; Gaillardet et al., 1999a), suggesting that the effect of carbonate weathering on the Sr isotopic composition of clays is probably minor. In addition, while one cannot exclude that atmospheric deposition can influence locally the $^{87}Sr/^{86}Sr$ composition of weathered mineral phases (*e.g.*, Pett-Ridge et al., 2009), it is also likely that any adsorbed Sr fraction associated with clay-size minerals would have been leached away during our sequential leaching procedure. To summarize, all the above consideration suggests that the combined influence of carbonate dissolution, rainwater and any other source effect in river catchments only plays a minor role in controlling the observed distribution of radiogenic Sr isotopes in studied fine-grained detrital fractions.

Finally, the presence of fine-grained sediments recycled from former sedimentary cycles also raises important concern about the utility of Sr isotopes in river sediments for tracing weathering processes. The geochemistry of suspended sediment loads in large river basins is indeed strongly influenced by the recycling of old sedimentary rocks (*e.g.*, Goldstein, 1988;

Gaillardet et al., 1999b; Dellinger et al., 2014). Despite this evidence, recent investigations of the same suite of river sediment samples have demonstrated clear correlations between proxies for silicate weathering and modern climatic parameters (Bayon et al., 2016; Bayon et al., 2018; Bayon et al., 2020a). For instance, in the Congo Basin, the Si isotopic composition (δ^{30}Si) of river clays transported in catchments dominated by sedimentary rocks exhibits strong relationships with precipitation levels in corresponding watersheds (Bayon et al., 2018). Similarly, in the Appalachians, the degree of weathering of the same Paleozoic shale formation along a latitudinal climate gradient also exhibits remarkable correlation with modern climatic parameters (Dere et al., 2013). Collectively, these multiple lines of evidence suggest that the weathered material eroded from catchments draining extensive areas of sedimentary rocks can still carry useful information on modern weathering conditions. In other words, this provides additional support to our working hypothesis that measured Sr isotopic ratios in paired clay- and silt-size fractions (and by inference Δ^{87}Sr/^{86}Sr $_{Clay-Silt}$) can be used to discuss about silicate weathering processes.

4.2. Δ^{87}Sr/^{86}Sr $_{Clay-Silt}$ as a proxy for silicate weathering intensity

As mentioned in the Results section, the observation that the degree of the size-dependent ^{87}Sr/^{86}Sr difference in studied sediments (Δ^{87}Sr/^{86}Sr $_{Clay-Silt}$) is more pronounced in river catchments draining ancient crystalline rocks can be explained by incongruent weathering processes. Upon rock formation, the radioactive decay of ^{87}Rb to ^{87}Sr results in a range of radiogenic Sr signatures among rock-forming minerals that progressively increases through geologic time. As a consequence, the alteration of 'old' silicate rocks can generate weathering products that have markedly different Sr isotopic compositions, while weathering of more recent rocks (such as basalts from recent volcanic provinces) results in secondary clays and residual detrital fractions with ^{87}Sr/^{86}Sr signatures that remain closer to the bulk rock

composition. On top of this age-dependency of radiogenic Sr isotope decoupling during

weathering processes, the degree of silicate weathering intensity also plays an important role

in controlling the distribution of $\Delta^{87}Sr/^{86}Sr_{\text{Clay-Silt}}$ in river sediments. This is suggested when

plotting $\Delta^{87}Sr/^{86}Sr_{\text{Clay-Silt}}$ against weathering indices (Fig. 6; Fig. 7), such as the chemical

index of alteration (CIA), the weathering index of Parker (WIP), and various elemental ratios

between mobile and immobile elements (Na_2O/Al_2O_3; $(MgO+K_2O)/Al_2O_3$). The CIA,

calculated in molar proportions as $[Al_2O_3/(Al_2O_3+CaO+Na_2O+K_2O)] \times 100$ (Nesbitt and

Young, 1982), provides a quantitative measure of the depletion of mobile (Ca, Na, K) versus

immobile (Al) elements during chemical weathering, which can be used as an estimate for the

degree of feldspar alteration in weathered rocks and sediments. Sediments and sedimentary

rocks exhibit a large range of CIA values, which depend on both the lithology of

corresponding source rocks and chemical weathering intensity (Nesbitt and Young, 1982).

The use of CIA and other weathering indices such as WIP in fine-grained fluvial sediments

generally reflects the integrated weathering history of drainage basins at the timescale of soil

formation (Li and Yang, 2010; Shao et al., 2012). In Fig. 6a,b, studied river sediments define

diffuse trends indicating more negative $\Delta^{87}Sr/^{86}Sr_{\text{Clay-Silt}}$ values as their CIA increases. The

observed correlation between CIA and the degree of size-dependent Sr isotopic decoupling in

river sediments is slightly improved when considering the CIA values of clays ($R^2=0.28$; $p \ll$

0.001) compared to silts ($R^2=0.22$; $p \ll 0.001$). Presumably, this could reflect the fact that silt-

size residual fractions contain a greater proportion of primary (unweathered) minerals,

meaning that their CIA is likely to be more strongly influenced by lithological effects rather

than by their degree of chemical alteration. While poorly to moderately weathered sediments

(with CIA $_{\text{clay}} < 75$) are systematically characterized by positive $\Delta^{87}Sr/^{86}Sr_{\text{Clay-Silt}}$ values (*e.g.*,

Lule and Ume rivers; Fig. 6a), more intensively weathered sediments (CIA $_{\text{clay}} > 75$)

commonly exhibit negative $\Delta^{87}Sr/^{86}Sr_{\text{Clay-Silt}}$ values (*e.g.*, Murchinson, Gascoyne, Kasai; Fig.

6a). Measured $\Delta^{87}Sr/^{86}Sr$ values also appear to yield similar relationships with the plagioclase index of alteration (PIA; calculated in molar proportions as $[(Al_2O_3 - K_2O)/(Al_2O_3+CaO+Na_2O - K_2O)] \times 100$; Fedo et al., 1995), with coefficient correlations (R^2) of 0.28 and 0.22 for clay- and silt-size fractions, respectively (plots not shown here). Amongst other commonly used weathering indices, WIP ($[(2Na_2O/0.35)+(MgO/0.9)+(2K_2O/0.25)+(CaO/0.7)] \times 100$, in molar proportions; Parker, 1970) is particularly useful when applied to heterogeneous parent rocks (Price and Velbel, 2003), providing a measure of the depletion in the most mobile major cations (Na, K, Mg, Ca) that takes into account their individual mobility in soils, based on their bond strengths with oxygen (Parker, 1970). In this study, $\Delta^{87}Sr/^{86}Sr_{Clay-Silt}$ and WIP display diffuse relationships, with correlation coefficients (R^2) of 0.18 ($p < 0.005$) and 0.33 ($p \ll 0.001$) in clay- and silt-size fractions, respectively (Fig. 6c,d). The slightly improved degree of correlation observed in river silts probably reflects the fact that WIP is most applicable to mildly leached primary detrital material (Price and Velbel, 2003), rather than to detrital fractions dominated by secondary clay mineral assemblages. In Fig. 6d, the silt-size fractions exhibiting the lowest WIP values (<20; *e.g.*, Murchinson, Kasai), hence showing the most pronounced degrees of mobile cation depletion, are typically associated with negative $\Delta^{87}Sr/^{86}Sr_{Clay-Silt}$ values.

To a large extent, the above mentioned general relationships between $\Delta^{87}Sr/^{86}Sr_{Clay-Silt}$ and weathering indices can be explained by considering both the relative partition coefficients (Kd) of Rb and Sr in rock-forming minerals and the respective susceptibility of different mineral phases to weathering (Fig. 1). In soils, secondary clay minerals are mostly derived from the alteration of ferromagnesian silicate minerals (clinopyroxene, amphibole, biotite) and feldspars (plagioclase, K-feldspar), characterized by relatively high and low Kd $_{Rb}$/ Kd $_{Sr}$ values, respectively (Fig. 1). Because biotite and other ferromagnesian minerals weather more

rapidly than feldspars, clay minerals formed in poorly to moderately weathered environments (*e.g.*, chlorite, illite, vermiculite) are expected to incorporate a radiogenic Sr isotopic signature compared to the corresponding residual silicate material. As chemical weathering intensifies, ferromagnesian minerals become depleted in soil profiles and the degree of feldspar weathering increases (*e.g.*, Nesbitt and Young, 1989), resulting in kaolinite-bearing mineral assemblages depleted in labile cations (Ca, Na, Mg, K) and presumably characterized by unradiogenic Sr signatures. This presumed relationship between $^{87}Sr/^{86}Sr$ and chemical weathering intensity in soils is generally well supported by field observations. For example, an investigation of glacial soil chronosequences in Wyoming documented a $^{87}Sr/^{86}Sr$ shift in both exchangeable and weathered mineral fractions towards less radiogenic signatures with increasing soil age, indicative of progressively intensifying weathering of unradiogenic plagioclase over biotite with time (Blum and Erel, 1997). In more intensively weathered soil sequences, the predominance of feldspar weathering is commonly associated with the presence of kaolinite characterized by low Sr isotopic compositions (*e.g.*, White et al., 2001; Pett-Ridge et al., 2009). While the degree of feldspar weathering probably largely accounts for the observed relationships between $\Delta^{87}Sr/^{86}Sr_{Clay-Silt}$ and weathering indices (Fig. 6; Fig. 7), the cause for the negative $\Delta^{87}Sr/^{86}Sr_{Clay-Silt}$ values observed in highly weathered environments remains unclear. Understanding the occurrence of such negative $\Delta^{87}Sr/^{86}Sr_{Clay-Silt}$ signatures requires identification of the mineral phases that are likely to drive residual silt fractions towards more radiogenic compositions than corresponding clays. We propose that this effect could be possibly explained by the particular behaviour of biotite in soils, which, unlike feldspars, weathers by a mechanism in which the primary phyllosilicate lattice is generally conserved (*e.g.*, Velbel, 1985; Kretzschmar et al., 1997). Altered grains of biotite are typically composed of a core of biotite, intertwined and surrounded by variable amounts of kaolinite, which may possibly act as a protective layer under intense weathering conditions

(*e.g.*, Kretzschmar et al., 1997; Murphy et al., 1998). This would be in agreement with previous evidence for the persistence of altered grains of biotite in highly weathered soil horizons, after all other primary minerals had completely weathered out (Pett-Ridge et al., 2009). Presumably, such kaolinite pseudomorphs of biotite could represent a substantial source of radiogenic Sr in the residual coarse fraction of tropical soils otherwise dominated by feldspar weathering, thereby possibly accounting for the observed negative $\Delta^{87}Sr/^{86}Sr_{Clay-Silt}$ in our study.

To some extent, the observed dispersion of $\Delta^{87}Sr/^{86}Sr_{Clay-Silt}$ in river sediments could also be partly controlled by the alteration of calcium and phosphate trace minerals in soils, such as sphene, apatite and allanite, which all display low Kd_{Rb}/Kd_{Sr} values (Fig. 1). In granitic environments, these accessory phases are dissolved during the early stages of chemical weathering (*e.g.*, Harlavan and Erel, 2002; Erel et al., 2004; Oliva et al., 2004), releasing substantial amounts of unradiogenic Sr in soil and river systems (*e.g.*, Aubert et al., 2001). In weathered soil sequences, apatite dissolution is typically followed by precipitation of more resistant secondary phosphate minerals, such as rhabdophane and florencite, which integrate elements previously released during early weathering stages, until more intense weathering conditions ultimately lead to their dissolution (*e.g.*, Banfield and Eggleton, 1989; Taunton et al., 2000; Oliva et al., 2004). Therefore, in addition to the relative contribution of biotite *versus* feldspar weathering, the successive phases of dissolution/precipitation of accessory phosphate minerals in soils could also possibly account for some of the observed size-dependent decoupling of Sr isotopes in river sediments.

4.3. Climatic and tectonic controls on $\Delta^{87}Sr/^{86}Sr_{Clay-Silt}$ in modern river sediments

Many earlier laboratory and field studies have provided evidence for the dependence of silicate mineral dissolution rates on climate and tectonics (*e.g.*, Velbel, 1993; Chen and Brantley, 1997; Murphy et al., 1998; Brantley et al., 1998; White et al., 1999; West et al., 2005; West, 2012; Dere et al., 2013; Li et al., 2016). The climatic and geomorphic characteristics of studied catchments can hence be used to further investigate the mechanisms controlling the size-dependent $^{87}Sr/^{86}Sr$ decoupling in modern river sediments worldwide. Amongst the various parameters affecting silicate weathering on continents (*e.g.*, temperature, precipitation, denudation rates, elevation, slope, soil thickness, curvature), we examine in Fig. 8 the relationships between $\Delta^{87}Sr/^{86}Sr_{Clay-Silt}$ and the mean annual temperature (MAT; Fig. 8a) and maximum basin elevation in studied catchments (Fig. 8b), which can be used, to a first approximation, as proxies for the climate and tectonic controls. Note that no particular relationships were found between $\Delta^{87}Sr/^{86}Sr_{Clay-Silt}$ and the catchment size of studied river basins (graph not shown here), meaning that the observed $\Delta^{87}Sr/^{86}Sr_{Clay-Silt}$ variability does not reflect any levelling effect that would occur on the geochemical signatures of suspended particulates in the largest river catchments. Of course, such a global approach suffers from inherent limitations due to the fact that major river basins commonly display large temperature gradients across their watershed between warm floodplains and cold high-elevation regions, such as for instance in the Amazon and the Himalayan river basins. Nevertheless, many studies have previously shown that the variability of weathering indices in river systems indicates significant relationships with MAT, providing useful information on the climatic control of chemical weathering in catchments (*e.g.*, Gaillardet et al., 1999a; Gaillardet et al., 2019; Li and Yang, 2010; Bayon et al., 2016, 2018, 2020a). In Fig. 8, a striking feature is that, except for two sediments from the Mackenzie River ($\Delta^{87}Sr/^{86}Sr_{Clay-Silt}$ = -0.002) and Elorn (-0.003), all the samples yielding negative $\Delta^{87}Sr/^{86}Sr_{Clay-Silt}$ correspond to tropical or sub-tropical river basins with MAT > 20°C. As discussed above, this finding is

best explained by enhanced alteration of feldspars under intense weathering conditions, resulting in the formation of kaolinite-bearing mineral assemblages characterized by unradiogenic Sr signatures. In contrast, the highest $\Delta^{87}Sr/^{86}Sr_{Clay-Silt}$ values (> +0.012) are encountered in sediments from sub-Arctic or temperate river basins with MAT < 10°C (Fig. 6). In cold and glacial environments, the alteration of biotite strongly dominates over feldspar weathering (*e.g.*, Blum et al., 1993; Anderson et al., 1997). As discussed above, this process results in the preferential release of dissolved radiogenic Sr signatures and the formation of weathered products characterized by high $^{87}Sr/^{86}Sr$ ratios (Blum et al., 1993; Blum and Erel, 1997). In this study, the same mechanism most likely accounts for the high $\Delta^{87}Sr/^{86}Sr_{Clay-Silt}$ values observed in most sub-Arctic rivers (Churchill, Nelson, Narva, Ume, Lule, Kymijoki). These observations are in full agreement with previous experimental works showing that at lower temperature, the initial cation release from biotite is significantly faster than cation release from plagioclase, and vice versa (White et al., 1999).

In addition to climate, tectonics also plays a major role in controlling silicate weathering rates in watersheds (*e.g.*, Raymo and Ruddiman, 1992; Riebe et al., 2001; Jacobson et al., 2003; West et al., 2005; West, 2012, Hartmann et al., 2014). High mountains are characterized by high physical erosion rates and thin soils, where kinetically-limited conditions generally reduce silicate weathering intensity. In high elevation environments, the rate of sediment supply is generally more rapid than silicate mineral dissolution, so that limited $^{87}Sr/^{86}Sr$ decoupling is expected to occur during weathering. In Fig. 8b, this is illustrated by the fact that all rivers draining areas of high topography (with maximum elevation > 4000 m; e.g. Ganges-Brahmaputra, Amu-Darya, Orinoco, Yukon, Amazon) display a very limited range of $\Delta^{87}Sr/^{86}Sr_{Clay-Silt}$ values (between +0.002 and +0.012). As elevation decreases, physical erosion rates decrease and soils thicken, leading to an increase in the proportion of silicate

mineral dissolution relative to sediment supply. In this context, enhanced silicate weathering can result in more pronounced decoupling of Sr isotopes between secondary clays and residual weathered products, as exemplified by the comparatively larger range of $\Delta^{87}Sr/^{86}Sr$ $_{Clay-Silt}$ (from -0.005 to +0.015) observed in the elevation range of 2000 to 4000 m (Fig. 8b). In Fig. 8b, the sediments exhibiting the most pronounced size-dependent $^{87}Sr/^{86}Sr$ decoupling (with $\Delta^{87}Sr/^{86}Sr$ $_{Clay-Silt}$ between -0.019 to +0.028) correspond to rivers draining areas of low topography (< 2000m), typically characterized by thick soil sequences and low denudation rates. In such transport-limited weathering regimes, the longer sediment residence time in soils leaves sufficient time for silicate mineral weathering to proceed. This implies that significant $^{87}Sr/^{86}Sr$ decoupling can occur between weathering products, leading either to mostly negative $\Delta^{87}Sr/^{86}Sr$ $_{Clay-Silt}$ in tropical regions dominated by feldspar weathering, or to positive $\Delta^{87}Sr/^{86}Sr$ $_{Clay-Silt}$ in sub-Arctic environments dominated by biotite alteration (Fig. 8b). Importantly, the proposed mechanism linking the degree of size-dependent $^{87}Sr/^{86}Sr$ decoupling in river sediments to the type of weathering regime in watersheds will be also dependent on the fact that ancient Precambrian shields are generally encountered in areas of low topography, while high elevation regions correspond to geologically young orogenic belts. This means that the observed trends between $\Delta^{87}Sr/^{86}Sr$ $_{Clay-Silt}$ and the maximum elevation in river basins are also crucially dependent on the age of the source rocks, hence representing a time-integrated relationship.

4.4. Regional and global solid fluxes of riverine Sr and $^{87}Sr/^{86}Sr$ to the ocean

Taken together, the cumulative area of the river basins investigated in this study accounts for a total of 37.5×10^6 km^2, hence representing about 35% of the entire continental area that drains into the global ocean (105×10^6 km^2; Milliman and Farnsworth, 2011). For each continental region (*e.g.*, Scandinavia, Western Europe, West Africa, East Asia), the largest

and/or most representative rivers were used to extrapolate regional solid fluxes of riverine Sr ($F_{Reg.}Sr$) and associated Sr isotopic composition $(^{87}Sr/^{86}Sr)_{Reg.}$ following the equations listed below:

$$F_{\mathrm{Re}g}Sr = \frac{\sum TSS_i.C_iSr}{\sum TSS_i} \times TSS_{\mathrm{Re}g}$$

$$\left(87Sr/86Sr\right)_{\mathrm{Re}g} = \frac{\sum TSS_i.C_iSr\left(87Sr/86Sr\right)_i}{\sum TSS_i.C_iSr}$$

where TSS_i, C_iSr and $(^{87}Sr/^{86}Sr)_i$ refer to the total suspended load (Mt/yr), Sr concentration and associated Sr isotopic compositions in either clay- or silt-size detrital fractions (µg/g) of individual river systems; and $TSS_{Reg.}$ represents the regional TSS value (Milliman and Farnsworth, 2011). An inherent uncertainty in this approach is the fact such regional Sr fluxes are strongly dependent on the $^{87}Sr/^{86}Sr$ and [Sr] values used for the largest river basins, where suspended particulate loads have been shown to display significant seasonal variability over the hydrological year (*e.g.*, Viers et al., 2008; Mao et al., 2011; Rousseau et al., 2019). As a consequence, the Sr regional fluxes calculated here should be only regarded as informative. Nevertheless, the significant $^{87}Sr/^{86}Sr$ seasonal variability previously identified in suspended particles from large river catchments can be generally ascribed, to a large extent, to a grain-size effect (*e.g.*, Bouchez et al., 2011). In this study, this effect is minimized because we analysed separate fractions of both clay-rich and silt-size detrital sediments. In addition, while the $^{87}Sr/^{86}Sr$ composition of suspended loads represents an instantaneous snapshot of the chemical composition of river particulates, fine-grained sediments deposited near the mouth of rivers integrate spatially-integrated source signatures over a much longer period of time. Therefore, we are confident that the approach described above can still provide indicative estimates of regional Sr fluxes worldwide. The obtained Sr fluxes are directly proportional to regional sediment yields (Table 3), indicating that about 40% of the solid Sr riverine flux to

the world ocean is derived from Indonesia and the Western Pacific area, followed by

contributions from South East Asia and the large Himalayan rivers (~25%) and northern

South America (~10%, corresponding mainly to the Amazon River). In Europe, the total

sediment flux to the ocean is dominated by inputs from Western Mediterranean regions,

which account for more than ~70% of associated solid Sr fluxes. during weathered

Collectively, our new global estimates for the total solid Sr fluxes from rivers to the ocean are

about 1.8 and 2.7 Mt/yr for river clays and silts, respectively (Table 3). The corresponding

average Sr concentration and ^{87}Sr/^{86}Sr of the clay- and silt-size detrital fractions, calculated

using the equations listed below, are 100 and 145 µg/g, and 0.7197 and 0.7156, respectively

(Table 3), which confirms that the river clays exported to the ocean are, at the global scale,

slightly more radiogenic than corresponding silts.

$$[Sr]Global = \frac{\sum_{Reg} TSS \times [Sr]Reg}{\sum_{Reg} TSS}$$

$$\left(\frac{87Sr}{86Sr}\right)Global = \frac{\sum_{Reg} TSS \times [Sr]Reg \times \left(\frac{87Sr}{86Sr}\right)Reg}{\sum_{Reg} TSS \times [Sr]Reg}$$

To the best of our knowledge, there are no estimates for the proportion of clays and silts

associated with the suspended particulate loads delivered to the ocean. Considering the

average proportion of each grain-size fraction in the studied river sediment samples (i.e. 85%

silts and 15% clays; Bayon et al., 2016), we can calculate a global ^{87}Sr/^{86}Sr composition of

0.7160 for the average river sediment exported to the ocean, being coincidently identical to

the value proposed more than 30 years ago by Goldstein and Jacobsen (1988).

5. Conclusions

This study presents new information about the factors controlling the distribution of

radiogenic strontium isotopes in river sediments. We show that the Sr isotopic difference

between clay- and silt-size fractions, termed here $\Delta^{87}Sr/^{86}Sr_{Clay-Silt}$, is related to the intensity of silicate weathering in river basins. The observed range of $\Delta^{87}Sr/^{86}Sr_{Clay-Silt}$ in river sediments worldwide largely reflects the temperature dependence of silicate weathering and its influence on the preferential alteration of radiogenic biotite *versus* unradiogenic feldspar in cold and warm environments, respectively. Our global survey for Sr isotopes in river sediments also suggests a link between $\Delta^{87}Sr/^{86}Sr_{Clay-Silt}$ and geomorphic parameters such as the maximum basin elevation, reflecting the fact that silicate weathering is most intense in areas of low topography, as opposed to high-mountain environments characterized by kinetically-limited weathering regimes. Future studies should now aim at assessing whether these findings hold true at the local scale, when investigating weathering profiles. Ultimately, the application of this new $\Delta^{87}Sr/^{86}Sr_{Clay-Silt}$ weathering proxy to sedimentary records could ideally complement the conventional use of radiogenic Sr isotopes as provenance tracers, thereby providing an unique set of geochemical tracers for reconstructing the evolution of past landscapes and silicate weathering over geologic times.

Acknowledgements

Declaration of interests

The authors declare that they have no known competing financial interests or personal relationships that could have appeared to influence the work reported in this paper.

Supplementary data

Supplementary material

References

Allègre, C., Dupré, B., Gaillardet, J., Négrel, P., 1996. Sr–Nd–Pb isotopes systematics in Amazon and Congo. Chem. Geol. 131, 93-112.

Armstrong, R.L., 1968. A model for the evolution of strontium and lead isotopes in a dynamic earth. Rev. Geophys. 6, 175-199.

Anderson, S.P., Drever, J.I., Humphrey, N.F., 1997. Chemical weathering in glacial environments. Geology 25, 399-402.

Asahara, Y., Tanaka, T., Kamioka, H., Nishimura, A., Yamazaki, T., 1999. Provenance of the north Pacific sediments and process of source material transport as derived from Rb–Sr isotopic systematics. Chem. Geol. 158, 271-291.

Aubert, D., Stille, P., Probst, A., 2001. REE fractionation during granite weathering and removal by waters and suspended loads: Sr and Nd isotopic evidence. Geochim. Cosmochim. Acta 65, 387-406.

Banfield, J.P., Eggleton, R.A., 1989. Apatite replacement and rare earth mobilization, fractionation and fixation during weathering. Clays Clay Miner. 37, 113-137.

Barrat, J.A., Keller, F., Amossé, J., Taylor, R.N., Nesbitt, R.W., Hirata, T., 1996. Determination of rare earth elements in sixteen silicate reference samples by ICP-MS after Tm addition and ion exchange separation. Geostand. Newslett. 20, 133-139.

Barrat, J.A., Zanda, B., Moynier, F., Bollinger, C., Liorzou, C., Bayon, G., 2012. Geochemistry of CI chondrites, Revisited: Major, Trace elements, Cu and Zn isotopes. Geochim. Cosmochim. Acta 83, 79-92.

Bayon, G., German, C.R., Boella, R.M., Milton, J.A., Taylor, R.N., Nesbitt, R.W., 2002. An improved method for extracting marine sediment fractions and its application to Sr and Nd isotopic analysis. Chem. Geol. 187, 179-199.

Bayon, G. et al., 2015. Rare earth elements and neodymium isotopes in world river sediments revisited. Geochim. Cosmochim. Acta 170, 17-38.

Bayon, G., Skonieczny, C., Delvigne, C., Toucanne, S., Bermell, S., Ponzevera, E., André, L., 2016. Environmental Hf-Nd isotopic decoupling in World river clays. Earth Planet. Sci. Lett. 438, 25-36.

Bayon, G., Delvigne, C., Ponzevera, E., Borges, A.V., Darchambeau, F., De Deckker, P., Lambert, T., Monin, L., Toucanne, S., André, L., 2018. The silicon isotopic composition of fine-grained river sediments and its relation to climate and lithology. Geochim. Cosmochim. Acta 229, 147-161.

Bayon, G., Lambert, T., Vigier, N., De Deckker, P., Freslon, N., Jang, K., Larkin, C., Piotrowski, A. M., Thollon, M., Tipper, E. T., 2020a. Rare earth element and neodymium isotope tracing of sedimentary rock weathering. Chem. Geol. 553, 119794.

Bayon, G., Douglas, G.B., Denton, G.J., Monin, L., De Deckker, P., 2020b. Preferential Riverine Export of Fine Volcanogenic Particles to the Southeast Australian Margin. Front. Mar. Sci. 7, 89.

Bindeman, I.N., Bayon, G., Palandri, J., 2019. Triple oxygen isotope investigation of fine-grained sediments from major world's rivers: Insights into weathering processes and global fluxes into the hydrosphere. Earth Planet. Sci. Lett. 528, 115851.

Biscaye, P.E., Dasch, E.J., 1971. The rubidium, strontium, strontium-isotope system in deep-sea sediments: Argentine Basin. J. Geophys. Res. 76, 5087-5096.

Blum, J.D., Erel, Y., 1995. A silicate weathering mechanism linking increases in marine $^{87}Sr/^{86}Sr$ with global glaciation. Nature 373, 415-418.

Blum, J.D., Erel, Y., 1997. Rb-Sr isotope systematics of a granitic soil chronosequence: The importance of biotite weathering. Geochim. Cosmochim. Acta 61, 3193-3204.

Blum, J.D., Erel, Y., Brown, K., 1993. $^{87}Sr/^{86}Sr$ ratios of Sierra Nevada stream waters: Implications for relative mineral weathering rates. Geochim. Cosmochim. Acta 57, 5019-5025.

Borg, L.E., Banner, J.L., 1996. Neodymium and strontium isotopic constraints on soil sources in Barbados, West Indies. Geochim. Cosmochim. Acta 60, 4193-4206.

Bouchez, J., Gaillardet, J., France-Lanord, C., Maurice, L., Dutra-Maia, P., 2011. Grain size control of river suspended sediment geochemistry: clues from Amazon River depth profiles. Geochem. Geophys. Geosyst.12, Q03008.

Brantley, S.L., Chesley, J.T., Stillings, L.L., 1998. Isotopic ratios and release rates of strontium measured from weathering feldspars. Geochim. Cosmochim. Acta 62, 1493-1500.

Brooks, C., 1968. Relationship between feldspar alteration and the precise post-crystallization movement of rubidium and strontium isotopes in a granite. J. Geophys. Res. 73, 4751-4757.

Capo, R.C., Stewart, B.W., Chadwick, O.A., 1998. Strontium isotopes as tracers of ecosystem processes: theory and methods. Geoderma 82, 197-225.

Mao, C., Chen, J., Yuan, X., Yang, Z., Ji, J., 2011. Seasonal variations in the Sr-Nd isotopic compositions of suspended particulate matter in the lower Changjiang River: Provenance and erosion constraints. Chin. Sci. Bull. 56, 2371-2378.

Chen, Y., Brantley, S.L., 1997. Temperature-and pH-dependence of albite dissolution rate at acid pH. Chem. Geol. 135, 275-290.

Clow, D.W., Mast, M.A., Bullen, T.D., Turk, J.T., 1997. Strontium 87/strontium 86 as a tracer of mineral weathering reactions and calcium sources in an alpine/subalpine watershed, Loch Vale, Colorado. Water Resour. Res. 33, 1335-1351.

Dasch,, E.J., 1969. Strontium isotopes in weathering profiles, deep-sea sediments, and sedimentary rocks. Geochim. Cosmochim. Acta 33, 1521-1552.

Dausmann, V., Gutjahr, M., Frank, M., Kouzmanov, K., Schaltegger, U., 2019. Experimental evidence for mineral-controlled release of radiogenic Nd, Hf and Pb isotopes from granitic rocks during progressive chemical weathering. Chem. Geol. 507, 64-84.

Dellinger, M., Gaillardet, J., Bouchez, J., Calmels, D., Galy, V., Hilton, R.G., Louvat, P., France-Lanord, C., 2014. Lithium isotopes in large rivers reveal the cannibalistic nature of modern continental weathering and erosion. Earth Planet. Sci. Lett. 401, 359-372.

Dere, A.L., White, T.S., April, R.H., Reynolds, B., Miller, T.E., Knapp, E.P., McKay, L.D., Brantley, S.L., 2013. Climate dependence of feldspar weathering in shale soils along a latitudinal gradient. Geochim. Cosmochim. Acta 122, 101-126.

Derry, L.A., France-Lanord, C., 1996. Neogene Himalayan weathering history and river $^{87}Sr/^{86}Sr$: impact on the marine Sr record. Earth Planet. Sci. Lett. 142, 59-74.

Dessert, C., Dupré, B., François, L.M., Schott, J., Gaillardet, J., Chakrapani, G., Bajpai, S., 2001. Erosion of Deccan Traps determined by river geochemistry: impact on the global climate and the $^{87}Sr/^{86}Sr$ ratio of seawater. Earth Planet. Sci. Lett. 188, 459-474.

Douglas, G.B., Gray, C.M., Hart, B.T., Beckett, R., 1995. A strontium isotopic investigation of the origin of suspended particulate matter (SPM) in the Murray-Darling River system, Australia. Geochim. Cosmochim. Acta 59, 3799-3815.

Dymond, J., Biscaye, P.E., Rex, R.W., 1974. Eolian origin of mica in Hawaiian soils. Geol. Soc. Am. Bull. 85, 37-40.

Eisenhauer, A., Meyer, H., Rachold, V., Tütken, T., Wiegand, B., Hansen, B.T., Spielhagen, R.F., Lindemann, F., Kassens, H., 1999. Grain size separation and sediment mixing in Arctic Ocean sediments: evidence from the strontium isotope systematic. Chem. Geol. 158, 173-188.

Erel, Y., Blum, J.D., Roueff, E., Ganor, J., 2004. Lead and strontium isotopes as monitors of experimental granitoid mineral dissolution. Geochim. Cosmochim. Acta 68, 4649-4663.

Faure, G., Hurley, P.M., 1963. The isotopic composition of strontium in oceanic and continental basalts: application to the origin of igneous rocks. J. Petrol. 4, 31-50.

Faure, G., Powell, J.L., 2012. Strontium isotope geology (Vol. 5). Springer Science & Business Media.

Fedo, C.M., Wayne, Nesbitt, H., Young, G.M., 1995. Unraveling the effects of potassium metasomatism in sedimentary rocks and paleosols, with implications for paleoweathering conditions and provenance. Geology 23, 921-924.

Franzese, A.M., Hemming, S.R., Goldstein, S.L., 2009. Use of strontium isotopes in detrital sediments to constrain the glacial position of the Agulhas Retroflection. Paleoceanography 24.

Gaillardet, J., Dupré, B., Allègre, C.J., 1997. Chemical and physical denudation in the Amazon river basin. Chem. Geol. 142, 141–173.

Gaillardet, J., Dupré, B., Louvat, P., Allègre, C.J., 1999a. Global silicate weathering and CO_2 consumption rates deduced from the chemistry of large rivers. Chem. Geol. 159, 3-30.

Gaillardet, J., Dupré, B., Allègre, C.J., 1999b. Geochemistry of large river suspended sediments: Silicate weathering or recycling tracer? Geochim. Cosmochim. Acta 63, 4037-4051.

Gaillardet, J., Calmels, D., Romero-Mujalli, G., Zakharova, E., Hartmann, J., 2019. Global climate control on carbonate weathering intensity. Chem. Geol. 527, 118762.

Galy, A., France-Lanord, C., 2001. Higher erosion rates in the Himalaya: Geochemical constraints on riverine fluxes. Geology 29, 23-26.

Garçon, M., Chauvel, C., 2014. Where is basalt in river sediments, and why does it matter?. Earth Planet. Sci. Lett. 407, 61-69.

Garçon, M., Chauvel, C., France-Lanord, C., Limonta, M., Garzanti, E., 2014. Which minerals control the Nd–Hf–Sr–Pb isotopic compositions of river sediments?. Chem. Geol. 364, 42-55.

Gast, P.W., 1960. Limitations on the composition of the upper mantle. J. Geophys. Res. 65, 1287-1297.

Gingele, F.X., De Deckker, P., 2005. Clay mineral, geochemical and Sr–Nd isotopic fingerprinting of sediments in the Murray–Darling fluvial system, southeast Australia. Aust. J. Earth Sci. 52, 965-974.

Goldstein, S.J., Jacobsen, S.B., 1987. The Nd and Sr isotopic systematics of river-water dissolved material: Implications for the sources of Nd and Sr in seawater. Chem. Geol. 46, 245-272.

Goldstein, S.J., Jacobsen, S.B., 1988. Nd and Sr isotopic systematics of river water suspended material: implications for crustal evolution. Earth Planet. Sci. Lett. 87, 249-265.

Goldstein, S.L., 1988. Decoupled evolution of Nd and Sr isotopes in the continental crust and the mantle. Nature 336, 733-738.

Grousset, F.E., Biscaye, P.E., 2005. Tracing dust sources and transport patterns using Sr, Nd and Pb isotopes. Chem. Geol. 222, 149-167.

Grousset, F.E., Biscaye, P.E., Zindler, A., Prospero, J., Chester, R., 1988. Neodymium isotopes as tracers in marine sediments and aerosols: North Atlantic. Earth Planet. Sci. Lett. 87, 367-378.

Hajj, F., Poszwa, A., Bouchez, J. Guérold, F., 2017. Radiogenic and "stable" strontium isotopes in provenance studies: A review and first results on archaeological wood from shipwrecks. J. Archaeol. Sci. 86, 24-49.

Harlavan, Y., Erel, Y., 2002. The release of Pb and REE from granitoids by the dissolution of accessory phases. Geochim. Cosmochim. Acta 66, 837-848.

Hartmann, J., Moosdorf, N., Lauerwald, R., Hinderer, M., West, A.J., 2014. Global chemical weathering and associated P-release—The role of lithology, temperature and soil properties. Chem. Geol. 363, 145-163.

Hemming, S.R., Van de Flierdt, T., Goldstein, S.L., Franzese, A.M., Roy, M., Gastineau, G., Landrot, G., 2007. Strontium isotope tracing of terrigenous sediment dispersal in the Antarctic Circumpolar Current: implications for constraining frontal positions. Geochem. Geophys. Geosyst. 8.

Jacobson, A.D., Blum, J.D., Chamberlain, C.P., Craw, D., Koons, P.O., 2003. Climatic and tectonic controls on chemical weathering in the New Zealand Southern Alps. Geochim. Cosmochim. Acta 67, 29-46.

Jochum, K.P., Weis, U. Schwager, B., Stoll, B., Wilson, S.A., Haug, G.H., Andreae, M.O. Enzweiler, J., 2016. Reference values following ISO guidelines for frequently requested rock reference materials. Geostand. Geoanal. Res. 40, 333-350.

Kretzschmar, R., Robarge, W.P., Amoozegar, A., Vepraskas, M.J., 1997. Biotite alteration to halloysite and kaolinite in soil-saprolite profiles developed from mica schist and granite gneiss. Geoderma 75, 155-170.

Krishnaswami, S., Trivedi, J. R., Sari, M.M., Ramesh, R., Sharma, K.K., 1992. Strontium isotopes and rubidium in the Ganga-Brahmaputra river system: Weathering in the

Himalaya, fluxes to the Bay of Bengal and contributions to the evolution of oceanic $^{87}Sr/^{86}Sr$. Earth Planet. Sci. Lett. 109, 243-253.

Li, C., Yang, S., 2010. Is chemical index of alteration (CIA) a reliable proxy for chemical weathering in global drainage basins?. Am. J. Sci. 310, 111-127.

Li, G., Hartmann, J., Derry, L.A., West, A.J., You, C.F., Long, X., Zhan, T., Li, L., Li, G., Qiu, W., Li, T., 2016. Temperature dependence of basalt weathering. Earth Planet. Sci. Lett. 443, 59-69.

McArthur, J.M., Howarth, R.J., Bailey, T.R., 2001. Strontium isotope stratigraphy: LOWESS version 3: best fit to the marine Sr-isotope curve for 0–509 Ma and accompanying look-up table for deriving numerical age. J. Geol. 109, 155-170.

McArthur, J.M., Howarth, R.J., Shields, G.A., 2012. Strontium isotope stratigraphy. The geologic time scale 1, 127-144.

Meyer, I., Davies, G.R., Stuut, J.B.W., 2011. Grain size control on Sr-Nd isotope provenance studies and impact on paleoclimate reconstructions: An example from deep-sea sediments offshore NW Africa. Geochem. Geophys. Geosyst. 12.

Miller, E.K., Blum, J.D., Friedland, A.J., 1993. Determination of soil exchangeable-cation loss and weathering rates using Sr isotopes. Nature 362, 438-441.

Milliman, J.D., Farnsworth, K.L., 2011. River Discharge to the Coastal Ocean, A global synthesis. Cambridge University Press, 392 pp.

Millot, R., Gaillardet, J., Dupré, B., Allègre, C.J., 2002. The global control of silicate weathering rates and the coupling with physical erosion: new insights from rivers of the Canadian Shield. Earth Planet. Sci. Lett.196, 83-98.

Murphy, S.F., Brantley, S.L., Blum, A.E., White, A.F., Dong, H., 1998. Chemical weathering in a tropical watershed, Luquillo Mountains, Puerto Rico: II. Rate and mechanism of biotite weathering. Geochim. Cosmochim. Acta 62, 227-243.

Nebel, O., Scherer, E.E., Mezger, K., 2011. Evaluation of the ^{87}Rb decay constant by age comparison against the U–Pb system. Earth Planet. Sci. Lett. 301, 1-8.

Négrel, P., 2006. Water-granite interaction: clues from strontium, neodymium and rare earth elements in soil and waters. Appl. Geochem. 21, 1432-1454.

Négrel, P., Allègre, C.J., Dupré, B., Lewin, E., 1993. Erosion sources determined from inversion of major, trace element and strontium isotopic ratios in river water: the Congo Basin case. Earth Planet. Sci. Lett. 120, 59-76.

Nesbitt, H.W., Young, G.M., 1982. Early Proterozoic climates and plate motions inferred from major element chemistry of lutites. Nature 299, 715-717.

Nesbitt, H.W., Young, G.M., 1989. Formation and diagenesis of weathering profiles. J. Geol. 97, 129-147.

Öhlander, B., Ingri, J., Land, M., Schöberg, H., 2000. Change of Sm-Nd isotope composition during weathering of till. Geochim. Cosmochim. Acta 64, 813-820.

Oliva, P., Dupré, B., Martin, F. Viers, J., 2004. The role of trace minerals in chemical weathering in a high-elevation granitic watershel (Estibere, France): chemical and mineralogical evidence. Geochim. Cosmochim. Acta 68, 2223-2243.

Palmer, M.R., Edmond, J.M., 1989. The strontium isotope budget of the modern ocean. Earth Planet. Sci. Lett. 92, 11-26.

Palmer, M.R., Edmond, J.M., 1992. Controls over the strontium isotope composition of river water. Geochim. Cosmochim. Acta 56, 2099-2111.

Parker, A., 1970. An index of weathering for silicate rocks. Geol. Mag. 107, 501-504.

Parra, M., Faugères, J.C. Grousset, F., Pujol, C., 1997. Sr-Nd isotopes as tracers of fine-grained detrital sediments: the South-Barbados accretionary prism during the last 150 kyr. Mar. Geol. 136, 225-243.

Pearce, C.R., Parkinson, I.J., Gaillardet, J., Charlier, B.L., Mokadem, F., Burton, K.W., 2015. Reassessing the stable ($\delta^{88/86}Sr$) and radiogenic ($^{87}Sr/^{86}Sr$) strontium isotopic composition of marine inputs. Geochim. Cosmochim. Acta 157, 125-146.

Pett-Ridge, J.C., Derry, L.A., Kurtz, A.C., 2009. Sr isotopes as a tracer of weathering processes and dust inputs in a tropical granitoid watershed, Luquillo Mountains, Puerto Rico. Geochim. Cosmochim. Acta 73, 25-43.

Peucker-Ehrenbrink, B., Fiske, G.J., 2019. A continental perspective of the seawater $^{87}Sr/^{86}Sr$ record: A review. Chem. Geol. 510, 140-165.

Pinet, P., Souriau, M., 1988. Continental erosion and large-scale relief. Tectonics 7, 563-582.

Price, J.R., Velbel, M.A., 2003. Chemical weathering indices applied to weathering profiles developed on heterogeneous felsic metamorphic parent rocks. Chem. Geol. 202, 397-416.

Probst, A., El Gh'mari, A., Aubert, D., Fritz, B., McNutt, R., 2000. Strontium as a tracer of weathering processes in a silicate catchment polluted by acid atmospheric inputs, Strengbach, France. Chem. Geol. 170, 203-219.

Raymo, M.E., Ruddiman, W.F., 1992. Tectonic forcing of late Cenozoic climate. Nature 359, 117-122.

Riebe, C.S., Kirchner, J.W., Granger, D.E., Finkel, R.C., 2001. Strong tectonic and weak climatic control of long-term chemical weathering rates. Geology 29, 511-514.

Rousseau, T.C., Roddaz, M., Moquet, J.S., Delgado, H.H., Calves, G., Bayon, G., 2019. Controls on the geochemistry of suspended sediments from large tropical South American rivers (Amazon, Orinoco and Maroni). Chem. Geol. 522, 38-54.

Shaffer, N.R., Faure, G., 1976. Regional variation of $^{87}Sr/^{86}Sr$ ratios and mineral compositions of sediment from the Ross Sea, Antarctica. Geol. Soc. Am. Bull. 87, 1491-1500.

Shao, J., Yang, S., Li, C., 2012. Chemical indices (CIA and WIP) as proxies for integrated chemical weathering in China: inferences from analysis of fluvial sediments. Sedim. Geol. 265, 110-120.

Singh, S.K., Kumar, A. France-Lanord, C., 2006. Sr and $^{87}Sr/^{86}Sr$ in waters and sediments of the Brahmaputra river system: silicate weathering, CO_2 consumption and Sr flux. Chem. Geol. 234, 308-320.

Singh, S.K., Rai, S.K., Krishnaswami, S., 2008. Sr and Nd isotopes in river sediments from the Ganga Basin: sediment provenance and spatial variability in physical erosion. J. Geophys. Res. Earth Surf. 113, doi.org/10.1029/2007JF000909

Stewart, B.W., Capo, R.C., Chadwick, O.A., 2001. Effects of rainfall on weathering rate, base cation provenance, and Sr isotope composition of Hawaiian soils. Geochim. Cosmochim. Acta 65, 1087-1099.

Taunton, A.E., Welch, S.A., Banfield, J.F., 2000. Microbial controls on phosphate and lanthanide distributions during granite weathering and soil formation. Chem. Geol. 169, 371-382.

Veizer, J., Compston, W., 1974. ^{87}Sr/^{86}Sr composition of seawater during the Phanerozoic. Geochim. Cosmochim. Acta 38, 1461-1484.

Veizer, J., 1989. Strontium isotopes in seawater through time. Annu. Rev. Earth Pl. Sc. 17, 141-167.

Velbel, M.A., 1985. Geochemical mass balances and weathering rates in forested watersheds of the southern Blue Ridge. Am. J. Sci. 285, 904-930.

Velbel, M.A., 1993. Temperature dependence of silicate weathering in nature: How strong a negative feedback on long-term accumulation of atmospheric CO2 and global greenhouse warming? Geology 21, 1059–1062.

Viers, J., Dupré, B., Braun, J.J., Deberdt, S., Angeletti, B., Ngoupayou, J.N., Michard, A., 2000. Major and trace element abundances, and strontium isotopes in the Nyong basin rivers (Cameroon): constraints on chemical weathering processes and elements transport mechanisms in humid tropical environments. Chem. Geol. 169, 211-241.

Viers, J. et al., 2008. Seasonal and provenance controls on Nd-Sr isotopic compositions of Amazon rivers suspended sediments and implications for Nd and Sr fluxes exported to the Atlantic Ocean. Earth Planet. Sci. Lett. 274, 511-523.

Walter, H.J., Hegner, E., Diekmann, B., Kuhn, G., 2000. Provenance and transport of terrigenous sediment in the South Atlantic Ocean and their relations to glacial and interglacial cycles: Nd and Sr isotopic evidence. Geochim. Cosmochim. Acta 64, 3813-3827.

Weis, D., Kieffer, B., Maerschalk, C., Pretorius, W., Barling, J., 2005. High-precision Pb-Sr-Nd-Hf isotopic characterization of USGS BHVO-1 and BHVO-2 reference materials. Geochem. Geophys. Geosyst. 6, doi:10.1029/2004GC000852

Weis, D. et al, 2006. High-precision isotopic characterization of USGS reference materials by TIMS and MC-ICP-MS. Geochem. Geophys. Geosyst. 7, doi.org/10.1029/2006GC001283

West, A.J., Galy, A., Bickle, M., 2005. Tectonic and climatic control on silicate weathering. Earth Planet. Sci. Lett. 235, 211-228.

West, A.J., 2012. Thickness of the chemical weathering zone and implications for erosional and climatic drivers of weathering and for carbon-cycle feedbacks. Geology 40, 811-814.

White, A.F., Blum, A.E., Bullen, T.D., Vivit, D.V., Schulz, M. Fitzpatrick, J., 1999. The effect of temperature on experimental and natural chemical weathering rates of granitoid rocks. Geochim. Cosmochim. Acta 63, 3277-3291.

White, A.F., Bullen, T.D., Schulz, M.S., Blum, A.E., Huntington, T.G., Peters, N.E., 2001. Differential rates of feldspar weathering in granitic regoliths. Geochim. Cosmochim. Acta 65, 847-869.

Wu, W., Xu, S., Yang, J., Yin, H., Tao, X., 2009. Sr fluxes and isotopic compositions in the headwaters of the Yangtze River, Tongtian River and Jinsha River originating from the Qinghai–Tibet Plateau. Chem. Geol. 260, 63-72.

Figure 1. The Rb-Sr mineral-liquid partition coefficient ratios (K_D) for most common granite-forming minerals and associated sequence of alteration. Partition coefficients were compiled from the GERM database (http://earthref.org/GERM) after removal of K_D values for rare rock types. The thin black line corresponds to the mean Rb/Sr partition coefficient ratio for each mineral. Darker shaded areas indicate Minimum, maximum and mean K_D values for the minerals reported in this plot are: apatite (0.002; 0.05; 0.026; n=2); allanite (0.037; 0.106; 0.071; n=2); clinopyroxene (0.018; 2.5; 0.35; n=32); amphibole (0.19; 2.23; 0.66; n=15); biotite (1.33; 38; 11.4; n=12); plagioclase (0.002; 0.19; 0.040; n=36); K-feldspar (0.03; 0.31; 0.17; n=9). The alteration of accessory calcium and phosphate mineral phases (*e.g.*, apatite, sphene, allanite) typically occur at

early stages of granitoid dissolution (*e.g.*, Harlavan and Erel, 2002; Erel et al., 2004; Oliva et al., 2004), followed by dissolution of ferromagnesian minerals (*e.g.*, clinopyroxene, amphibole, biotite). More resistant K-feldspars weather under intense weathering conditions, associated with the release of unradiogenic dissolved Sr fraction (with relatively low $^{87}Sr/^{86}Sr$).

Figure 2. The location of studied sediment samples and corresponding river basins. Yellow triangles and green diamonds correspond to rivers from ancient cratons and other areas dominated by igneous/metamorphic crystalline basement rocks, and volcanic watersheds, respectively. Black circles indicate rivers draining mixed and sedimentary rock formations.

Figure 3. Pseudo-isochron Rb-Sr diagrams in river sediments. (a) $^{87}Sr/^{86}Sr$ *versus* Rb/Sr in studied clay- and silt-size detrital fractions, indicating a positive relationship in mixed/sedimentary basins (with a best-fit regression line of $R^2 = 0.38$; excluding the samples from the Fitzroy, Narva and Nelson rivers), which reflects both the average age of the upper continental crust drained in river catchments and a grain-size effect. (b) $^{87}Sr/^{86}Sr$ *versus* Rb/Sr in selected paired clay- and silt-size fractions. While most paired size fractions display typical pseudo-isochrons, a few river sediment samples exhibit inverse grain-size relationships (dashed lines) with clay fractions being characterized by lower $^{87}Sr/^{86}Sr$ and higher Rb/Sr values than corresponding silts.

Figure 4. Neodymium and strontium isotopes in river sediments. (a) ε_{Nd} *versus* $^{87}Sr/^{86}Sr$ in studied clay- and silt-size detrital fractions, displaying typical inverse relationships. For comparison is shown a set of Nd-Sr isotopic data for various granites, basalts and

Archaean rocks complied from the GEOROC database (http://georoc.mpch-
mainz.gwdg.de/georoc/). Note that Nd isotopic data are from previous studies (Bayon et
al., 2015; 2016; 2019). (b) ε_{Nd} *versus* $\Delta^{87}Sr/^{86}Sr_{Clay-Silt}$, which represents the $^{87}Sr/^{86}Sr$
difference between paired clay- and silt-size fractions in river sediments. The observed
range of $\Delta^{87}Sr/^{86}Sr_{Clay-Silt}$ is larger in river catchments dominated by old crystalline rocks
characterized by unradiogenic Nd isotopic signatures (between -0.019 to +0.028), than in
rivers draining mixed/sedimentary basins (from -0.011 to +0.015) and volcanic provinces
(< +0.004). This reflects the age dependency of the radiogenic Sr isotope decoupling
between different grain sizes.

Figure 5. The relationship between $\Delta^{87}Sr/^{86}Sr_{Clay-Silt}$ and $\Delta\varepsilon_{Nd\ Clay-Silt}$ in river sediments. In
mixed/sedimentary basins, the samples characterized by $\Delta\varepsilon_{Nd\ Clay-Silt} > 1$ are generally
interpreted as reflecting the preferential presence of fine volcanogenic particles in clay-
size fractions relative to corresponding silts (Bayon et al., 2015). In crystalline
basements, the size-dependent Nd isotope decoupling in those samples with $\Delta\varepsilon_{Nd\ Clay-Silt} <$
1 is most likely caused by incongruent silicate weathering (Öhlander et al., 2000;
Dausmann et al., 2019). The absence of any significant correlation between size-
dependent Nd and Sr isotope decoupling suggests that the observed $\Delta^{87}Sr/^{86}Sr$ variability
in river sediments is not controlled by a source effect. The vertical yellow band indicates
the range of $\Delta\varepsilon_{Nd\ Clay-Silt}$ values < |1| for which both clay- and silt-size fractions are
expected to derive from the same sediment sources.

Figure 6. The relationships between $\Delta^{87}Sr/^{86}Sr_{Clay-Silt}$ and chemical weathering indices in
river clays and silts. (a,b) $\Delta^{87}Sr/^{86}Sr_{Clay-Silt}$ *versus* the chemical index of alteration (CIA).
(c,d) $\Delta^{87}Sr/^{86}Sr_{Clay-Silt}$ *versus* the weathering index of Parker (WIP). Both river clays and

silts define diffuse trends indicating more negative $\Delta^{87}Sr/^{86}Sr$ $_{Clay\text{-}Silt}$ values as their degree of alteration increases. Poorly to moderately weathered sediments (with CIA $_{clay}$ < 75) are characterized by positive $\Delta^{87}Sr/^{86}Sr$ $_{Clay\text{-}Silt}$ values, while more intensively weathered sediments (CIA $_{clay}$ > 75) commonly exhibit negative $\Delta^{87}Sr/^{86}Sr$ $_{Clay\text{-}Silt}$ values.

Figure 7. $\Delta^{87}Sr/^{86}Sr$ $_{Clay\text{-}Silt}$ *versus* major element ratios in clays: (a) Na_2O/Al_2O_3 and (b) $(MgO+K_2O)/Al_2O_3$. The observed positive relationships suggest the link between the size-dependent Sr isotopic decoupling in river sediments and the intensity of silicate weathering, which results in the progressive depletion of mobile elements (Na, Mg, K) relative to immobile elements such as Al. In soils, the early alteration of amphibole and biotite (enriched in K and Mg) leads to formation of clay minerals that incorporate a radiogenic Sr isotopic signature compared to the corresponding residual silicate material. As chemical weathering intensifies, the degree of feldspar weathering increases, resulting in kaolinite-bearing mineral assemblages characterized by low Na_2O_2/Al_2O_3 ratios and unradiogenic Sr signatures.

Figure 8. Relationships between $\Delta^{87}Sr/^{86}Sr$ $_{Clay\text{-}Silt}$ and selected basin characteristics for (a) climate (mean annual temperature, MAT) and (b) topography (maximum basin elevation). In cold regions (MAT < 10°C), positive $\Delta^{87}Sr/^{86}Sr$ $_{Clay\text{-}Silt}$ indicate preferential alteration of biotite in soils, while in warm environments (MAT > 20°C), intense feldspar weathering results in negative $\Delta^{87}Sr/^{86}Sr$ $_{Clay\text{-}Silt}$. The degree of size-dependent Sr isotope decoupling is also more pronounced in low-elevation environments (< 2000 m), where transport-limited conditions are typically associated with intense silicate weathering processes, than in high mountain regions (> 4000m) dominated by kinetically-limited weathering regimes.

Table 1. Sr isotopic compositions of clay- and silt-size detrital fractions in river sediments.

	River	Type	Area (10³km²)	Lat. (°N)	Long. (°E)	MAT (°C)	Max elev. (m)	$^{87}Sr/^{86}Sr$ clay ± 2 se		Sr clay (ppm)	Rb clay (ppm)	$^{87}Sr/^{86}Sr$ silt ± 2 se		Sr silt (ppm)	Rb silt (ppm)
Rivers draining crystalline basements															
1	Congo	Margin	3800	-5.70	11.23	23.9	1760	0.745035	± 8	42	88	0.756287	± 10	52	102
2	Kasai (* Congo)	SPM	890	-3.18	16.20	23.5	1550	0.744120	± 11	19	16	0.753739	± 11	34	21
3	Lualaba (* Congo)	SPM	1035	0.60	24.80	22.2	4250	0.764651	± 49	38	96	0.754644	± 10	91	142
4	Niger	Margin	2200	3.20	6.68	29.4	1340	0.722114	± 8	67	163	0.716456	± 10	260	108
5	Benue (* Niger)	River	305	7.86	6.89	26.6	1340	0.720564	± 9	93	189	0.715904	± 8	269	106
6	Orinoco	River	1100	7.65	-66.18	23.9	6000	0.740648	a	64	a	0.734340	± 11	57	53
7	Rio Caroni (* Orinoco)	River	95	8.33	-62.71	25.0	2660	0.786745	± 15	53	72	0.779570	± 9	69	90
8	Rio Caura (*Orinoco)	River	48	7.58	-64.94	25.0	2350	0.7??728	± 12	58	77	0.785338	± 10	68	91
9	Rio Aro (* Orinoco)	River	30	7.39	-64.01	25.0	810	0.??209?	± 11	24	57	0.760058	± 7	81	69
10	Churchill	Estuary	290	58.97	-94.10	-3.0	860	0.744?73	± 8	227	161	0.730543	± 8	290	87
11	Murchinson	River	82	-27.83	114.69	22.0	71?	0.???074	± 9	63	124	0.777882	± 10	36	54
12	Gascoyne	River	79	-29.83	113.77	22.0	5?4	0.749595	± 9	61	122	0.766852	± 9	80	94
13	Fortescue	River	50	-21.29	116.14	25.1	?15?	0.800699	± 14	31	85	0.791301	± 9	40	72
14	Kymijoki	Estuary	37	60.46	26.91	3.0	?00	0.765864	± 11	111	165	0.751964	± 12	144	143
15	Ume	Estuary	26	63.72	20.27	1.?	?00	0.763772	± 9	85	153	0.735794	± 11	189	100
16	Lule	River	25	65.68	21.82	-2.?	?00	0.749513	± 10	99	133	0.729469	± 8	256	92
17	East Alligator	River	14	-12.43	132.97	?3	480	0.724718	± 10	66	108	0.735708	± #	33	27
18	Betsiboka	Margin	12	-15.52	45.72	26.3	940	0.713964	± 9	68	52	0.717193	± 12	126	70
19	Elorn	Estuary	0.3	48.40	-4.3?	?1	340	0.724731	± 9	104	184	0.727313	± 10	86	104
Rivers draining volcanic provinces															
20	Brantas	River	11.8	-7.44	12.4?	25	3480	0.705372	± 12	34	12	0.705160	± 10	35	12
21	River Maine	River	0.3	54.??	-6.32	8.7	460	0.706737	± 14	46	7	0.704979	± 9	136	8
22	Six Mile River	River	0.3	54.70	-6.15	8.7	420	0.711056	± 9	44	20	0.707455	± 13	124	17
Rivers draining mixed/sedimentary basins															
23	Amazon	Sub delta	6300	3.??	-49.50	26.7	5500	0.726631	± 10	92	163	0.722333	± 10	135	129
24	Mississipi	Sub delta	3300	2?.??	-89.49	12.8	3700	0.726629	± 10	70	154	0.722969	± 10	110	99
25	Nile	Margin	2900	?2.?1	30.38	26.7	3800	0.713491	± 8	115	92	0.715455	± 8	141	72
26	Parana	River	2?00	-27.47	-58.86	21.1	4800	0.738986	± 9	79	188	0.728374	± 8	74	63
27	Yangtze	Estuary	1?00	31.62	121.01	15.6	3200	0.729454	± 10	72	212	0.723176	± 8	116	142
28	Mackenzie	Sub delta	1800	69.26	-137.29	-3.3	3600	0.727033	± 7	133	191	0.728817	± 9	99	110
29	Ganges-Brahmaputra	Delta	16?0	23.17	90.47	18.3	7000	0.746839	± 17	80	213	0.735326	± 10	140	110
30	Brahmaputra (* G-B)	Delta	?70	24.91	89.78	15.0	5500	0.729109	± 10	103	235	0.727080	± 8	163	161
31	Volga	Estuary	1400	45.71	47.92	3.8	600					0.715912	± 10	142	63
32	Nelson	Estuary	1100	57.39	-91.80	-3.0	3400	0.742330	± 9	208	164	0.727383	± 8	241	71
33	Murray	River	1100	-35.41	139.23	18.3	2200	0.724560	b	84	b	0.721599	± 10	61	124
34	Yukon	River	850	61.93	-162.88	-5.1	6000	0.716103	± 9	150	124	0.708781	± 9	221	32
35	Danube	River	820	45.06	29.62	10.0	4100	0.723907	± 9	65	177	0.718675	± 10	102	92
36	Mekong	Delta	800	10.96	105.06	21.1	5100	0.722977	± 9	70	175	0.718744	± 8	69	61
37	Yellow River	Delta	750	37.80	118.91	12.8	3100	0.727390	± 32	73	150	0.717307	± 8	163	84
38	Amu Darya	River	535	42.22	60.12	8.8	6990	0.718455	± 9	103	147	0.712903	± 13	185	62
39	Don	River	420	47.29	39.10	6.8	180	0.718970	± 10	77	130	0.718179	± 10	104	51
40	Northern Dvina	Estuary	357	65.09	39.00	0.6	200	0.733683	± 8	125	142	0.729567	± 8	137	109
41	Fraser	Margin	230	49.16	-123.37	4.4	4000	0.710757	± 17	101	75	0.709104	± 7	252	64
42	Rhine	Estuary	220	51.91	4.48	8.1	3500	0.723074	± 9	75	199	0.718736	± 10	83	85
43	Vistula	Gulf	200	54.65	19.28	7.6	2500	0.758240	± 20	56	181	0.750031	± 10	79	134
44	Red River	Delta	160	20.26	106.52	24.0	3100	0.733489	± 7	91	223	0.737989	± 10	73	136
45	Chao Phraya	Delta	160	13.57	100.58	28	2500	0.714750	± 9	125	175	0.719568	± 9	68	109
46	Loire (Port-Lavigne)	Estuary	120	47.20	-1.64	10.9	1900	0.723349	± 10	61	166	0.716021	± 9	164	139
47	Loire (Donges)	Estuary	'	47.30	-2.07	'	'	0.723702	± 10	81	218	0.716528	± 12	161	151
48	Loire (Cordemais)	Estuary	'	47.28	-1.89	'	'	0.723558	± 11	83	217	0.715955	± 8	172	137
49	West Fitzroy	River	86	-17.73	123.64	19.0	490	0.791683	± 10	49	156	0.786724	± 10	70	122
50	Seine	River	79	49.47	0.42	13	900	0.725631	± 9	77	183	0.723558	± 9	78	60
51	Fly River	Estuary	76	-8.67	144.00	26.2	4000	0.712928	± 9	116	126	0.711739	± 8	139	86
52	Sepik	Margin	78	-3.13	142.78	25.0	4000	0.709698	± 8	105	86	0.706465	± 8	186	53
53	Narva	Estuary	56	59.54	27.58	5.5	320	0.775341	± 10	85	180	0.761562	± 10	100	134
54	Mae Klong	River	31	13.43	99.95	28.0	2200	0.746881	± 12	34	256	0.747546	± 10	33	191
55	Shannon	Estuary	23	52.69	-8.91	9	570	0.738141	± 21	80	207	0.725672	± 8	61	51

56	Adour	River	16	43.49	-1.47	13.0	2800	0.717362	±	9	159	209	0.716208	±	10	107	66
57	Sefid Rud	River	13	-12.43	132.97	14.0	4230	0.712471	±	10	118	121	0.708193	±	11	225	76
58	Lower River Bann	River	5.8	37.47	49.94	8.7	640	0.726947	±	9	57	87	0.716825	±	9	95	48
59	Mayenne	River	4.4	54.86	-6.48	12	420	0.735049	±	9	70	171	0.731434	±	8	71	105
60	River Blackwater	River	1.1	47.50	-0.55	8.7	360	0.733693	±	10	46	123	0.719380	±	10	107	54
61	Moyola River	River	0.3	54.51	-6.58	8.7	540	0.734450	±	12	67	132	0.729770	±	10	99	87
				54.75	-6.52												

* Tributary of a larger river system. Mean annual temperatures (MAT) are from Pinet and

Souriau (1988) or from the CLIMWAT climatic database. Maximum elevation are from

Milliman and Farnsworth (2011) or calculated from GIS (Bayon et al., 2020a). a) Parra et

al. (1997). b) Gingele and De Deckker (2005).

Table 2. Sr isotopic compositions of the NIST 987 standard and rock reference materials.

Standard	Measured ^{87}Sr/^{86}Sr			Reference ^{87}Sr/^{86}Sr			
	± 2 sd		N		± 2 sd		Ref
NIST-987	######	±	9	3?	######	±	12	Weis et al. (2005)
BHVO-2	######	±	15	?0	######	±	19	Weis et al. (2006)
BIR-1	######	±	19	8	######	±	26	Jochum et al. (2016)
BCR-1	######	±	15	10	######	±	19	Weis et al. (2006)
BCR-2	######	±	14	10	######	±	16	Weis et al. (2006)

Regions	Representative rivers used for regional estimates	TSS	CLAYS			SILTS		
			Sr flux		^{87}Sr/^{86}Sr	Sr flux		^{87}Sr/^{86}Sr
		(Mt/yr)	(t/yr)	(µg/g)			(µg/g)	
America								
	American Arctic	Mackenzie, Nelson, Churchill	270	41,732	155	0.7329	37,896	140	0.7285
	E. North America	Mississippi	630	44,063	70	0.7266	69,391	110	0.7230
	Western Americas	Yukon, Fraser	1,530	1,36,822	137	0.7150	2,29,128	229	0.7089
	N.E. South America	Amazon, Orinoco	1,600	2,09,338	93	0.7289	2,68,198	124	0.7232
	S. South America	Parana	120	9,529	79	0.7390	8,846	74	0.7284
Africa								
	W. Africa	Congo, Niger	550	29,657	54	0.7358	83,585	152	0.7235
	E. Africa	Nile	400	45,808	115	0.7135	56,265	141	0.7155
Eurasian Arctic / Russia	Northern Dvina, Volga	150	17,125	114	0.7222	21,100	141	0.7202
Europe								
	Scandinavia	Narva, Kymijoki, Ume, Lule	20	1,753	88	0.7720	1,752	88	0.7538
	W. Europe	Rhine, Loire, Vistula, Seine	25	1,781	71	0.7333	2,168	87	0.7296
	Iceland	Maine	48	2,197	46	0.7067	6,519	136	0.7050
	Black Sea	Danube, Don	140	9,120	65	0.7237	14,353	103	0.7187

	Western Med. Sea	Adour	620	98,590	159	0.7174	66,557	107	0.7162
S.E. Asia									
	E. Asia	Yangtze, Mekong, Red, Yellow, Chao Phraya	2,500	1,85,997	74	0.7277	3,41,001	136	0.7193
	E. Himalaya	Amu-Darya	500	51,338	103	0.7185	92,678	185	0.7129
	Bay of Bengal	Ganges, Brahmaputra	2,100	1,93,558	92	0.7367	3,18,828	152	0.7308
Indonesia & W. Pacific		Fly, Sepik, Brantas	7,230	7,54,228	104	0.7112	########	152	0.7087
Australia		Murray, Fitzroy, East Alligator	170	12,810	75	0.7290	9,765	57	0.7352
World Rivers			######	18,45,000	100	0.7197	########	145	0.7156

Global riverine fluxes of Sr to the ocean	(Mt/yr)	(µg/g)	$^{87}Sr/^{86}Sr$
Detrital load (This study; 85% silts - 25% clays)	2.52	138	0.7160
Suspended load (Goldstein and Jacobsen, 1988)	2.9.	221	0.7160
Dissolved load (Peucker-Ehrenbrink and Fiske, 2019)	⸳.ᵢ⸳	0.10	0.7111
Dissolved load (Goldstein and Jacobsen, 1987)	⸳.52	0.06	0.7101

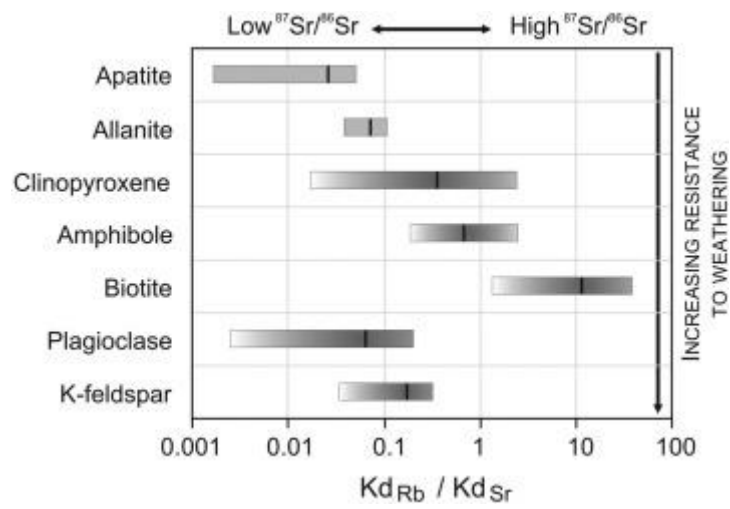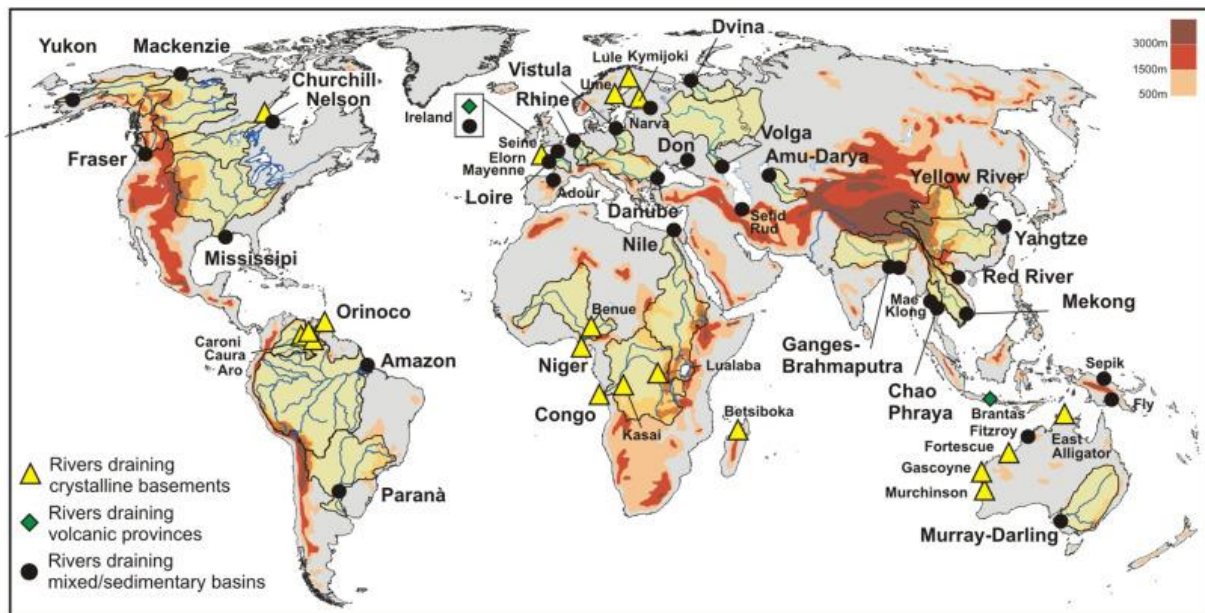**Table 3.** Regional and global solid fluxes of riverine Sr and $^{87}Sr/^{86}Sr$ to the ocean.
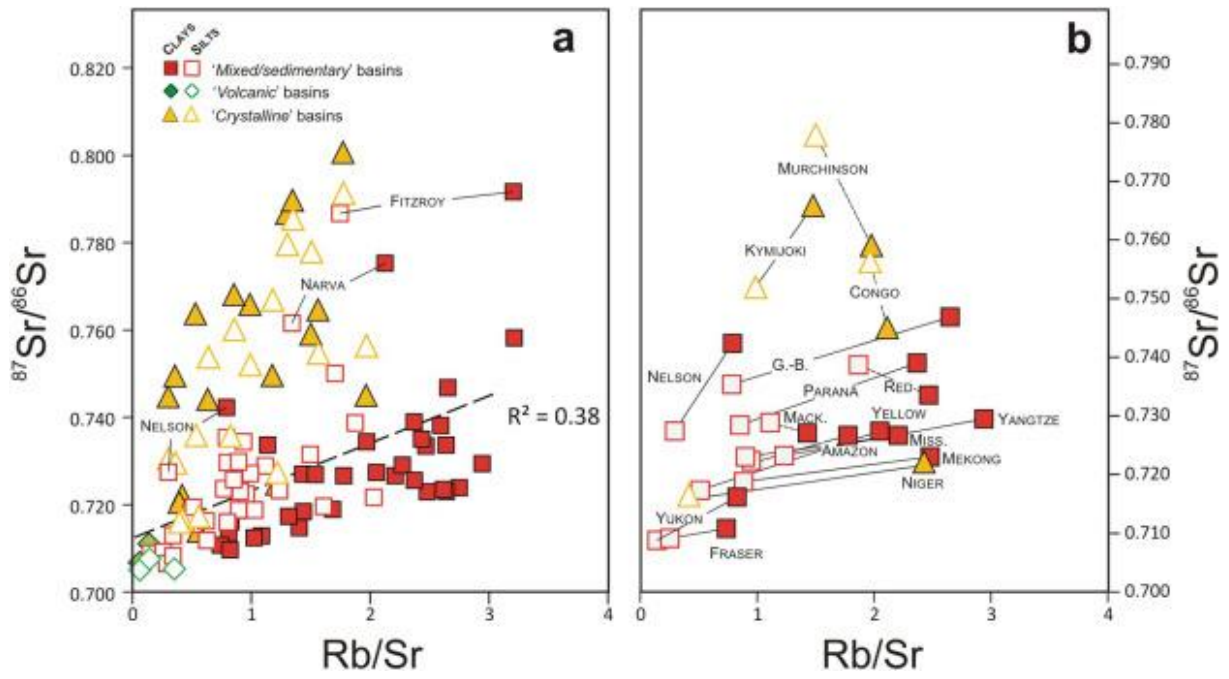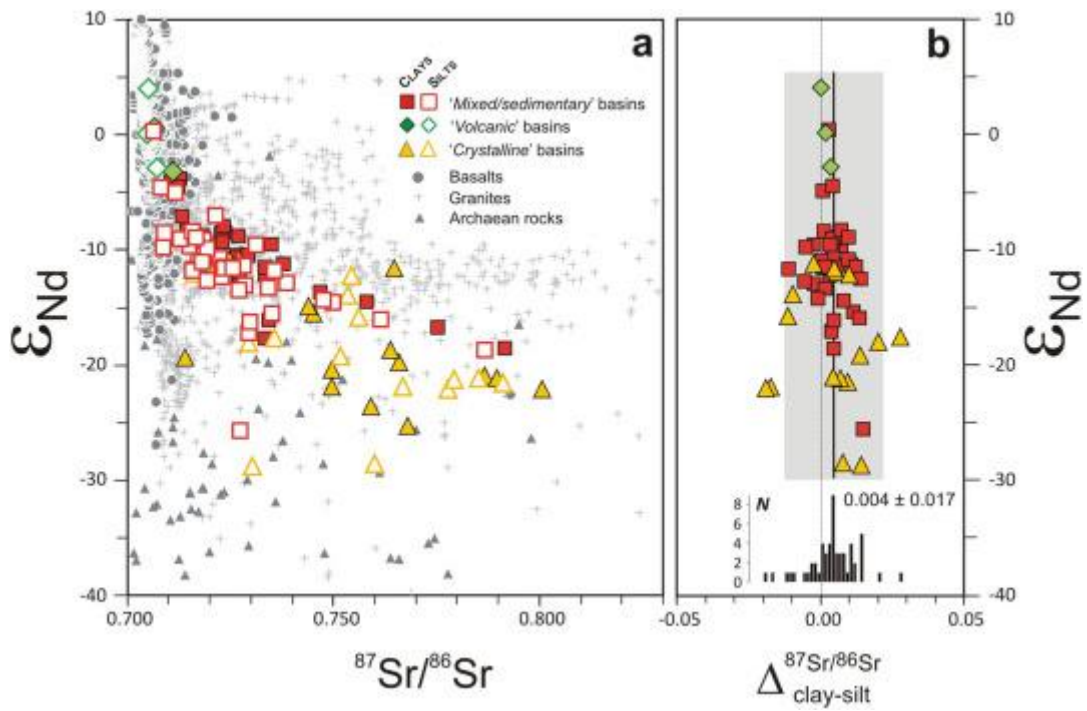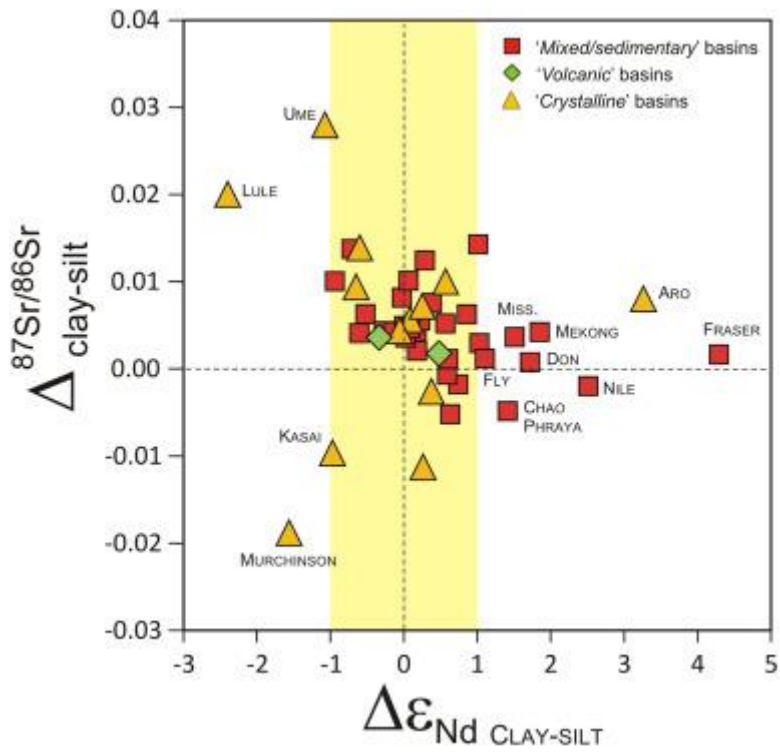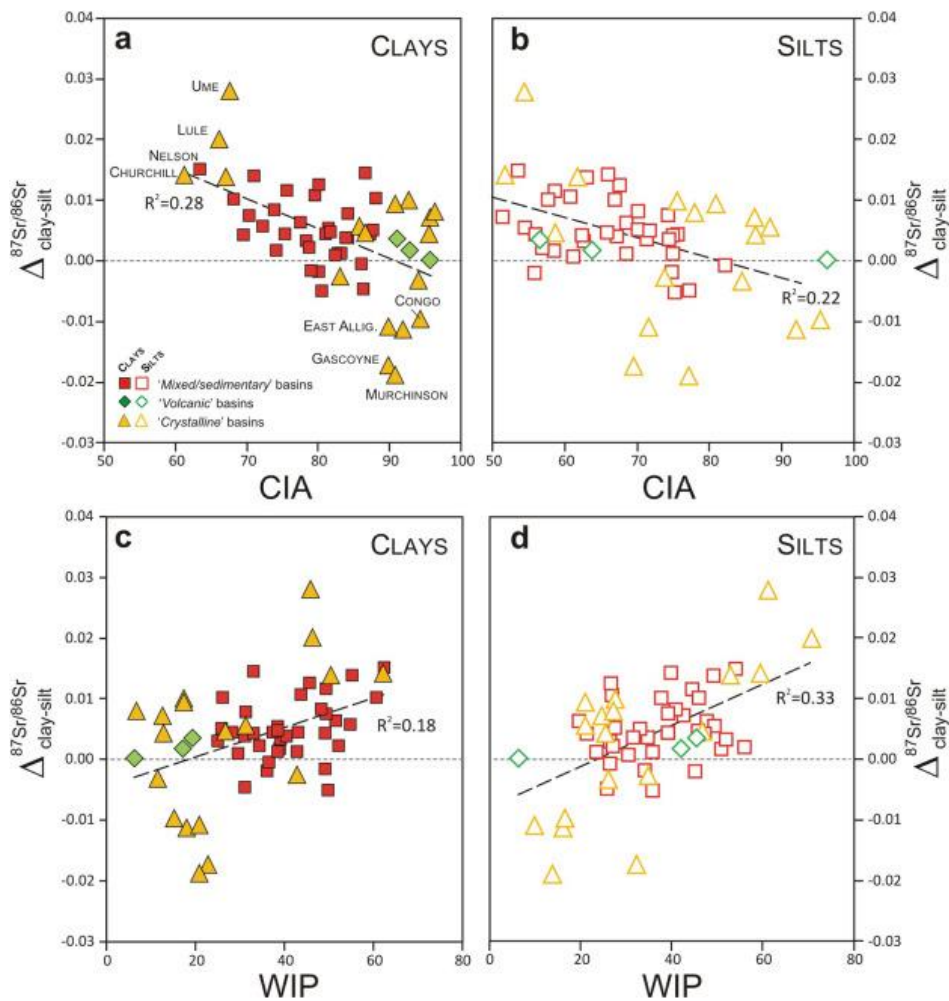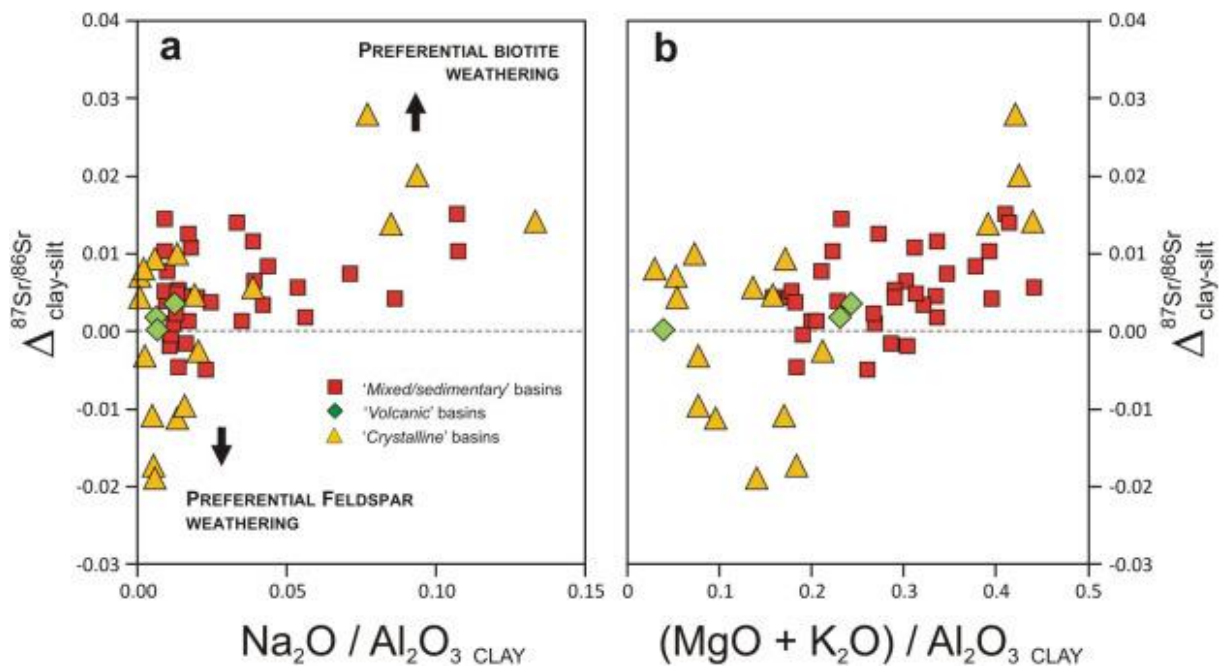
Figure 1

Figure 2

Figure 3

Figure 4

Figure 5

Figure 6

Figure 7

Figure 8